ACS OMEGA

http://pubs.acs.org/journal/acsodf

Article

Discrete Singular Metallophilic Interaction in Stable Large 12-Membered Binuclear Silver and Gold Metallamacrocycles of Amido-Functionalized Imidazole and 1,2,4-Triazole-Derived N-Heterocyclic Carbenes

A. P. Prakasham,[†] Sagar K. Patil,[†] Chandrasekhar Nettem,[†] Shreyata Dey, Gopalan Rajaraman,* and Prasenjit Ghosh*

Cite This: *ACS Omega* 2023, 8, 6439−6454

Read Online

ACCESS | Metrics & More | Article Recommendations | Supporting Information

ABSTRACT: Metallophilic interactions were observed in four pairs of 12-membered metallamacrocyclic silver and gold complexes of imidazole-derived N-heterocyclic carbenes (NHCs), [1-(R^1)-3-N-(2,6-di-(R^2)-phenylacetamido)-imidazol-2-ylidene]$_2M_2$ [R^1 = *p*-MeC_6H_4, R^2 = Me, M = Ag (**1b**) and Au (**1c**); R^1 = Me, R^2 = *i*-Pr, M = Ag (**2b**) and Au (**2c**); R^1 = Et, R^2 = *i*-Pr, M = Ag (**3b**) and Au (**3c**)], and a 1,2,4-triazole-derived N-heterocyclic carbene (NHC), [1-(*i*-Pr)-4-N-(2,6-di-(*i*-Pr)-phenylacetamido)-1,2,4-triazol-2-ylidene]$_2M_2$ [M = Ag (**4b**) and Au (**4c**)]. The X-ray diffraction, photoluminescence, and computational studies indicate the presence of metallophilic interactions in these complexes, which are significantly influenced by the sterics and the electronics of the N-amido substituents of the NHC ligands. The argentophilic interaction in the silver **1b**−**4b** complexes was stronger than the aurophilic interaction in the gold **1c**−**4c** complexes, with the metallophilic interaction decreasing in the order **4b** > **1b** > **1c** > **4c** > **3b** > **3c** > **2b** > **2c**. The **1b**−**4b** complexes were synthesized from the corresponding amido-functionalized imidazolium chloride **1a**−**3a** and the 1,2,4-triazolium chloride **4a** salts upon treatment with Ag_2O. The reaction of **1b**−**4b** complexes with $(Me_2S)AuCl$ gave the gold **1c**−**4c** complexes.

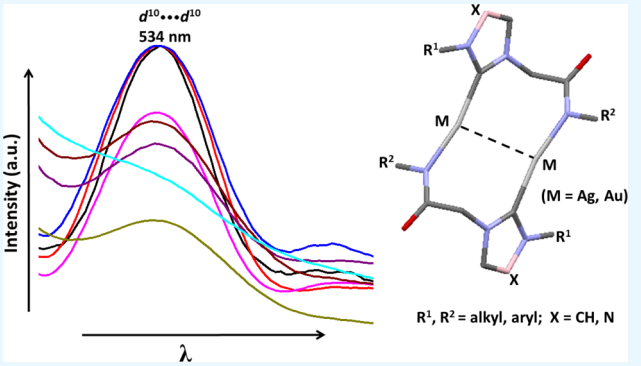

INTRODUCTION

The closed-shell···closed-shell metallophilic interactions,[1,2] commonly seen in coinage metals like Au, Ag, and Cu, are of interest in recent times mainly for their high-end material applications,[3] in crystal engineering,[4] supramolecular chemistry,[5] etc.[6,7] Apart from being the focus of mere intellectual curiosity, owing to strange aggregations due to bonding interactions between the coinage metal cations with closed-shell d^{10} configurations, these metallophilic interactions also arise interest for their photoluminescence,[8] electrical conductivity,[9,10] and other unexpected properties.[7] The aurophilic interaction, being the most common, has been most extensively studied,[11,12] followed by the argentophilic and cuprophilic interactions.[13] These metallophilicities are weak interactions akin to hydrogen bonding, $\pi-\pi$ stacking, ion−ion, ion−dipole, and dipole−dipole interactions. They can have similar profound implications in supramolecular and material applications if exploited judiciously.

The metallophilic interactions, are recognized primarily from the observed short metal···metal contacts, which can also be an artifact of ligand and lattice constraints. Hence, an accurate assessment of the interaction comes from their photoluminescence properties, aided by computational insights. The presence of weak metallophilic interactions is invoked for a long range of metal···metal separations of up to ca. 4 Å,[2,14] particularly due to the lack of clarity on the true values of the van der Waals radius of the coinage metals like silver and gold.[15] For example, the van der Waals radius of silver varies from that of the Bondi's estimate of 1.72 Å[16] to that of 2.1 Å by Batsanov[17] or from that of the Bondi's[16] van der Waals radius of 1.66 Å for gold to that of 2.1 Å by Batsanov.[17] The metallophilic interactions are ubiquitous in silver and gold complexes containing bridging[18] and nonbridging ligands.[19,20]

Since the appearance of the first systematic investigations of the Au(I)···Au(I) interactions 4 decades ago,[21−23] the concept of metallophilicity has been the subject of intense discussions with the understanding of its true nature continuing to

Received: October 19, 2022
Accepted: January 31, 2023
Published: February 9, 2023

Downloaded via INDIAN INST OF TECH BOMBAY on May 27, 2023 at 14:34:37 (UTC).
See https://pubs.acs.org/sharingguidelines for options on how to legitimately share published articles.

© 2023 The Authors. Published by American Chemical Society

evolve.[2,7,24−27] The crucial involvement of metal···metal dispersion interactions in rendering stability to these metallophilic aggregates was shown by the breakdown of the interaction energy, with a minimal influence of the ligands on the overall interaction profile.[28] Magnko calculated the $\{(PH_3)AuCl\}_2$ dimer's potential well depth to be −34.82 kJ/mol at an Au···Au distance of 3.025 Å in line with Pyykkö's earlier estimation.[29] The orbital pairs belonging to the gold *d*-shell were the principal contributors to the correlation energy. Further, it was demonstrated that, in the case of the Cu(I) and Ag(I) complexes, the correlation contributions involving the ligand orbitals solely could play a significantly more prominent role.[30] In this series of the dimeric $\{(PH_3)MCl\}_2$ (M = Cu, Ag, Au) examples, the strength of the metallophilic interaction was estimated to increase from Cu (−22.09 kJ/mol) to Ag (−30.70 kJ/mol) and to Au (−34.82 kJ/mol).[30] However, using CCSD(T) calculations, Kaltsoyannis showed that the strength of the metallophilic interaction maximized at Ag and weakened further down group 11.[31] In this context, our objective was to shed further light on the observed pattern by adding new synthesized examples, containing discrete singular metallophilic interactions, to the ongoing discussion about understanding the true nature of the d^{10}−d^{10} interactions.

A primary challenge for studying these interactions arises from their unrestricted extended aggregated nature, which seriously restricts designing systems with discrete singular interactions for a comprehensive study of the metallophilic interaction.[10,22] These interactions are ubiquitous and can be mainly manipulated with supported and unsupported ligand systems in designing supramolecular assemblies.[6,10,23] However, the approach to design complexes exhibiting discrete singular metallophilic interactions remains a formidable task with fewer examples prevalent in the literature.[19,21,32−34]

The weak but persistent metallophilic interaction manifests in aggregated structures extending from complex supramolecular assemblies to polynuclear motifs of all varieties.[6] Ligands with different steric, electronic, and coordinating requirements stabilize these interactions in various aggregated motifs. The intermolecular metallophilic interactions are more common and observed for many bridging and nonbridging ligands. The intramolecular version is, however, comparatively fewer in number and poses a more significant challenge in their design and synthesis, primarily for reasons of containing the metallophilic interaction within the molecule and from preventing it to extend beyond in intermolecular fashion.

With our interest in understanding the metallophilic interaction, particularly in the ones stabilized over the N-heterocyclic carbenes, we have reported several examples of the metallophilicity bearing supported[32,33] and unsupported ligands.[19] Here, in this manuscript, we report four pairs of silver **1b**−**4b** and gold **1c**−**4c** N-heterocyclic carbene complexes (Figure 1) derived from imidazole and 1,2,4-triazole rings, bearing discrete singular intramolecular metallophilic interactions. The combined photoluminescence and computational studies provide valuable insights into the nature of the metallophilic interactions in these complexes.

RESULTS AND DISCUSSION

A class of amido-functionalized imidazole **1a**−**3a** and 1,2,4-triazole (**4a**)-based N-heterocyclic carbene ligand precursors were synthesized from the corresponding 1-R^1-imidazole (R^1 = 4-MeC_6H_4, Me, Et) and 1-(*i*-Pr)-1,2,4-triazole by the direct alkylation with 2-chloro-N-2,6-$(R^2)_2$-phenylacetamide (R^2 = Me, *i*-Pr) (Scheme 1). The formations of these imidazole-based **1a**−**3a** and 1,2,4-triazole (**4a**)-based N-heterocyclic carbene ligand precursors were evident from the appearance of the characteristic highly downfield-shifted NC*H*N resonance at δ ca. 10.05−10.53 ppm for the imidazole-based **1a**−**3a** ligand precursors and at 11.26 ppm for the 1,2,4-triazole-based **4a** ligand precursor in the ^{1}H NMR spectra (Figures S1, S24, S49, and S74). The subsequent reaction of the N-heterocyclic carbene precursors **1a**−**4a** with Ag_2O yielded the corresponding large 12-membered silver **1b**−**4b** metallamacrocycles, the formation of which was supported by the observation of the Ag−$C_{carbene}$ resonances at δ ca. 177.2−182.3 ppm in the $^{13}C\{^1H\}$ NMR spectra (Figures S10, S33, S58, and S83).

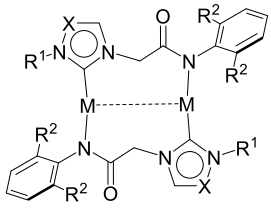

R^1 = *p*-$CH_3C_6H_4$, R^2 = Me, X = CH; M = Ag (**1b**), Au(**1c**)
R^1 = Me, R^2 = *i*-Pr, X = CH; M = Ag (**2b**), Au (**2c**)
R^1 = Et, R^2 = *i*-Pr, X = CH; M = Ag (**3b**), Au (**3c**)
R^1 = R^2 = *i*-Pr, X = N; M = Ag (**4b**), Au (**4c**)

Figure 1. Twelve-membered metallamacrocyclic silver **1b**−**4b** and gold **1c**−**4c** complexes exhibiting discrete metallophilic interactions.

The molecular structures of the **1b**−**4b** complexes, as determined using a single-crystal X-ray diffraction technique, revealed the large 12-membered metallamacrocyclic nature of these complexes (Figures 2, S14, S37, and S62 and Table S1). These structures display C_i symmetry. The Ag−$C_{carbene}$ bond lengths of 2.071(2) Å (**1b**), 2.059(2) Å (**2b**), 2.0621(17) Å (**3b**), and 2.054(8) Å (**4b**) are comparable to the related analogues reported in the literature.[32,33] Similarly, the Ag−N_{amido} bond distances were 2.0971(16) Å in **1b**, 2.0831(15) Å in **2b**, 2.0911(13) Å in **3b**, and 2.124(6) Å in **4b**, and a near-linear bond angle [∠C(1)−Ag(1)−N(3) (°)] was observed at the metal center [167.90(7) in (**1b**), 170.01(6) in (**2b**), 166.36(6) in (**3b**), and 176.1(3) in (**4b**)].

Interestingly, all of the 12-membered metallamacrocyclic silver **1b**−**4b** complexes indicated the existence of argentophilic interaction in these complexes as observed from the short Ag···Ag distances of 3.1061(3) Å in (**1b**), 3.6495(4) Å in (**2b**), 3.3810(4) Å in (**3b**), and 2.9974(8) Å in (**4b**). These Ag···Ag distances are within the range obtained by twice the van der Waals radius of Ag that varied from the estimate of 1.72 Å by Bondi[16] to that of 2.1 Å by Batsanov.[17]

The large 12-membered gold macrometallacyclic analogues **1c**−**4c** were conveniently obtained from the silver **1b**−**4b** complexes by the treatment with $(SMe_2)AuCl$ (Scheme 1). In $^{13}C\{^1H\}$ NMR, the Au−$C_{carbene}$ resonances of **1c**−**4c**, appeared at δ ca. 168.9−172.1 ppm, upfield-shifted from the Ag−$C_{carbene}$ resonances of δ ca. 177.2−182.3 ppm observed in case of **1b**−**4b** (Figures S10, S17, S33, S40, S58, S65, S83, and S89). Quite significantly, unlike the silver **1b**−**4b** complexes, all of the gold **1c**−**4c** complexes were characterized by the high-resolution mass spectroscopy (HRMS) measurements in which the molecular ion (M^+) peak appeared at *m*/*z* 1031.2615 for **1c** (calculated *m*/*z* 1031.2617), *m*/*z* 1013.3067 for **2c** (calculated *m*/*z* 1013.3062), *m*/*z*

https://doi.org/10.1021/acsomega.2c06729
ACS Omega 2023, 8, 6439−6454

Scheme 1. Synthetic Route to Amido-Functionalized Ag–NHC 1b–4b and Au–NHC 1c–4c Complexes

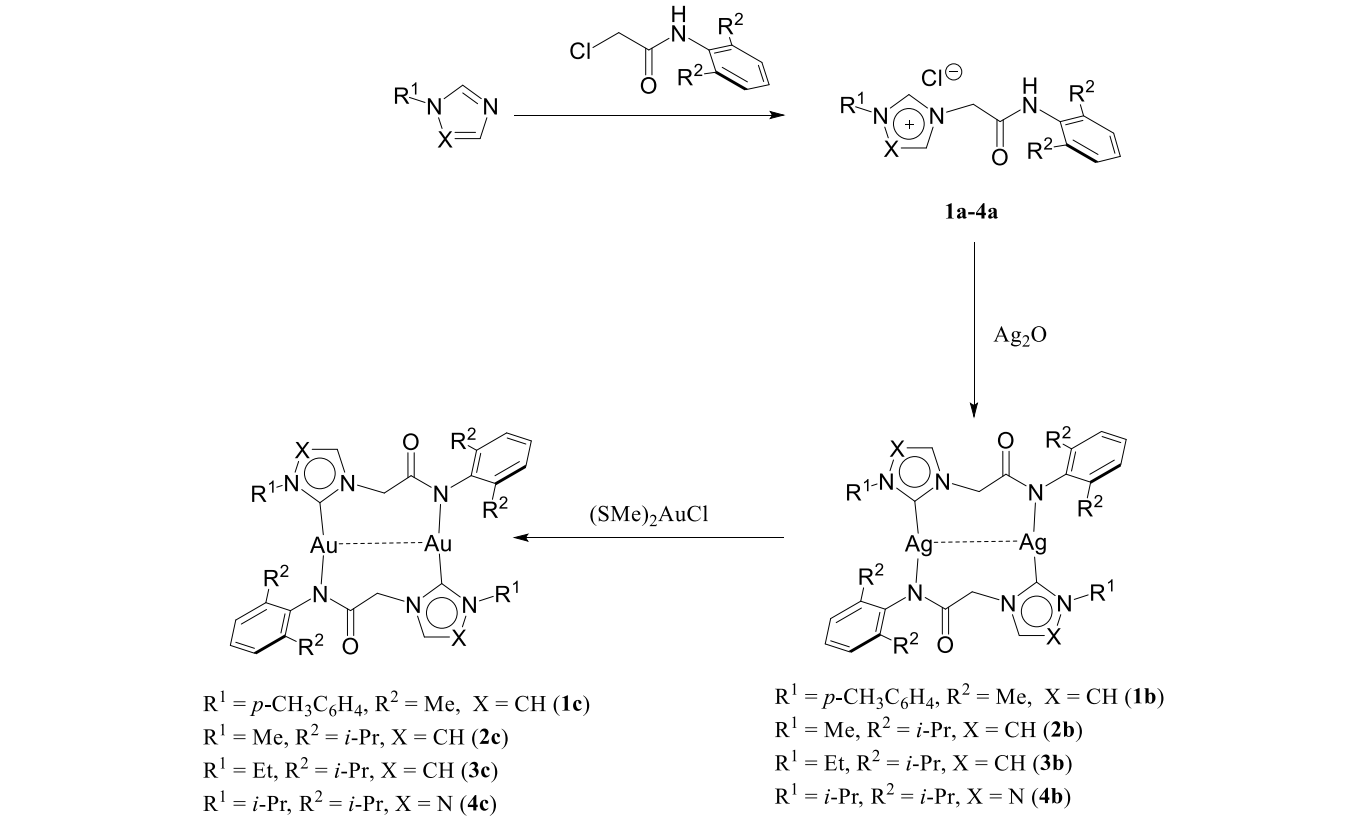

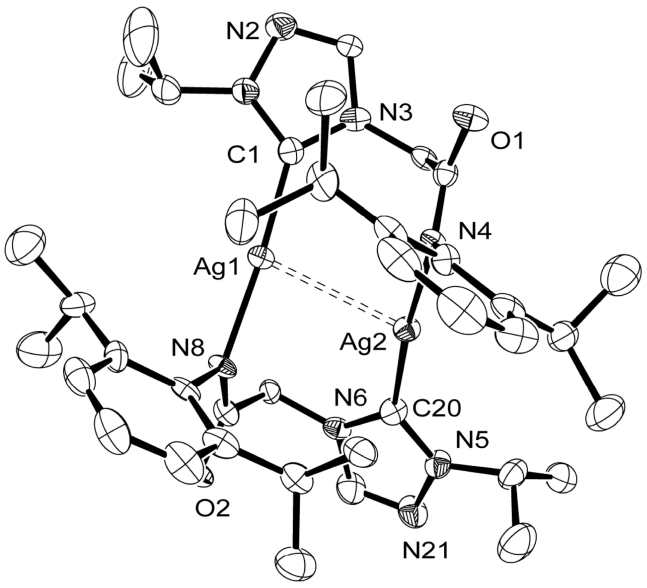

Figure 2. ORTEP of **4b** with thermal ellipsoids shown at the 50% probability level. Hydrogen atoms and cocrystallized CH_3CN molecules are omitted for clarity. Selected bond lengths (Å) and angles (°): Ag(1)···Ag(2) 2.9974(8), Ag(1)–C(1) 2.054(8), Ag(1)–N(8) 2.125(6), C(1)–N(1) 1.382(10), C(1)–N(3) 1.361(10), C(1)–Ag(1)–N(8) 176.1(3), C(1)–Ag(1)–Ag(2) 100.7(2), N(1)–C(1)–N(3) 100.7(7), N(3)–C(1)–Ag(1) 132.3(6), and N(1)–C(1)–Ag(1) 127.0(6).

1019.3553 for **3c** (calculated *m/z* 1019.3556), and *m/z* 1049.3770 for **4c** (calculated *m/z* 1049.3774) (Figures S20, S43, S68, and S92).

The gold **1c–4c** complexes were isostructural with their silver analogues **1b–4b** (Figures 3, S22, S45, and S70 and Table S1) as observed from the single-crystal X-ray diffraction studies. The gold structures display C_i symmetry. The Au–$C_{carbene}$ bond lengths of 1.993(2) Å (**1c**), 1.996(3) Å (**2c**),

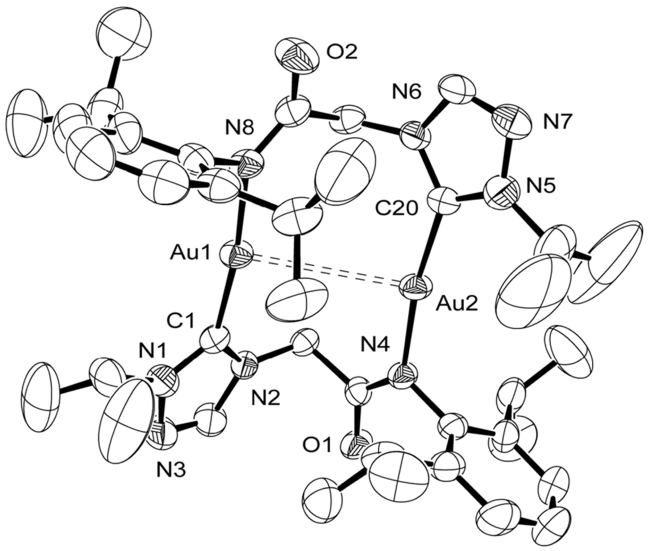

Figure 3. ORTEP of **4c** with thermal ellipsoids shown at the 50% probability level. Hydrogen atoms and cocrystallized H_2O molecule were omitted for clarity. Selected bond lengths (Å) and angles (°): Au(1)···Au(2) 3.5640(5), Au(1)–C(1) 1.975(4), Au(1)–N(8) 2.031(3), C(1)–N(1) 1.330(5), C(1)–N(2) 1.361(5), C(1)–Au(1)–N(8) 172.00(14), N(1)–C(1)–N(2) 103.4(3), N(2)–C(1)–Au(1) 130.5(3), and N(1)–C(1)–Au(1) 126.1(3).

https://doi.org/10.1021/acsomega.2c06729
ACS Omega 2023, 8, 6439–6454

1.985(4) Å (**3c**), and 1.975(4) Å (**4c**) are shorter than their silver analogues [2.071(2) Å (**1b**), 2.059(2) Å (**2b**), 2.0621(17) Å (**3b**), and 2.054(8) Å (**4b**)] due to smaller covalent radii of Au (1.37 Å)[35] compared to Ag (1.46 Å).[35] Quite interestingly, except for the **2c** complex, in which a longer Au···Au contact of 4.2597(8) Å was observed, the remaining gold complexes displayed a much shorter metal··· metal contact of 3.3462(2) Å (**1c**), 3.6358(5) Å (**3c**), and 3.5640(5) Å (**4c**).

The photoluminescence studies indicated that both of the silver **1b−4b** and the gold **1c−4c** complexes exhibited metallophilic interactions in solution and in the solid state at room temperature. For the silver **1b−4b** complexes, the excitation at 242 nm (λ) gave the Ag···Ag emission band at ca. 533−534 nm in $CHCl_3$ solution and at ca. 549−559 in the solid state at room temperature (Table 1 and Figures 4, 5, S23, S46−S48, S71−S73, and S94−S96). The other high-energy band at ca. 430 nm for **1b** (Figure 4), 433 nm for **2b** (Figure S46), 446 nm for **3b** (Figure S71), and 431 nm for **4b** (Figure S94) in $CHCl_3$ solution has been assigned to the ligand-based transitions, while in the solid state, the same emission was observed at ca. 389−390 nm for **1b−4b** (Figures 5, S23, S47, S48, S72, S73, S95, and S96). Similarly, the presence of aurophilic interactions in **1c−4c** was evident from the photoluminescence experiments, which too displayed a low-energy emission band at ca.530−533 nm in $CHCl_3$ (Table 1 and Figures 4, S46, S71, and S94) and at ca. 548−559 nm in the solid state at room temperature (Figures 5, S23, S47, S48, S72, S73, S95, and S96). Like the silver **1b−4b** complexes, the ligand-based high-energy band appeared at ca. 433 nm for **1c**, 427 nm for **2c**, 431 nm for **3c**, and 430 nm for **4c** in $CHCl_3$ and at ca. 389−390 nm for **1c−4c** in the solid state.

Table 1. Absorption and Emission Data for NHC Ligand Precursors 1a−4a, the Silver 1b−4b, and the Gold 1c−4c Complexes

		room temperature	
compounds	λ_{abs}, nm (ε_{max}, L^s mol^{-1} cm^{-1})	λ_{em}, nm in $CHCl_3$	λ_{em}, nm in solid state
1a	242 (28 504)	375	389
1b	239 (34 429)	430, 534	389, 549
1c	238 (62 451)	433, 532	390, 548
2a	240 (2645)	425	390
2b	240 (5683)	433, 534	389, 553
2c	250 (92 708)	427, 533	389, 552
3a	240 (3676)	426	389
3b	240 (7765)	446, 533	390, 559
3c	254 (54 145)	431, 532	389, 559
4a	240 (3008)	421	390
4b	239 (5868)	431, 534	389, 552
4c	238 (10 093)	430, 530	389, 552

The metal···metal distances in the silver **1b−4b** and the gold **1c−4c** complexes and their emission bands compared well with other related structurally characterized large 12-membered metallamacrocycles known in the literature (Tables 2 and 3).[32,33] It is worth mentioning that all of the structurally characterized examples of such large 12-membered silver and gold metallamacrocycles of amido-functionalized imidazole and 1,2,4-triazole-derived N-heterocyclic carbenes have been reported from our group[32,33] with four complexes of the each metals being part of the current study (Tables 2 and 3).

The density functional theory (DFT) studies were undertaken to understand the electronic structures of the silver **1b−4b** and the gold **1c−4c** complexes. The metallophilic interactions were looked at by performing topological analysis, and the noncovalent interaction calculations were done for the visualization of the interactions between the silver and the gold atoms. The electron localization functions were estimated to understand electron localization between two metal atoms. In this regard, it is worth mentioning that, as the secondary interactions like hydrogen bonding, $\pi-\pi$ stacking, and the crystal packing effects are more dominant over a weaker cuprophilic interactions[13] than the relatively stronger argento-philic and aurophilic interactions,[10,11,27] these secondary interactions are considered to have no significant influence in the metallophilic interactions in the silver **1b−4b** and the gold **1c−4c** complexes for the computational study.

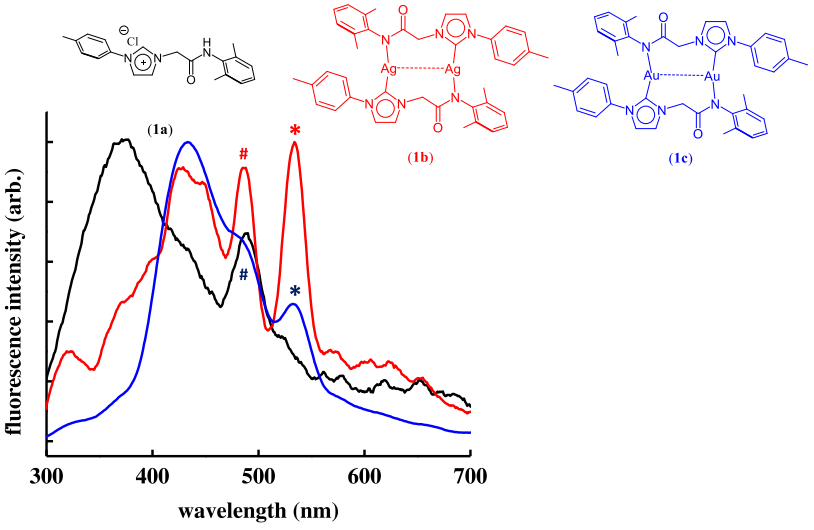

Figure 4. Comparison of the emission spectra of the ligand (**1a**), the Ag−NHC complex (**1b**), and the Au−NHC complex (**1c**) in $CHCl_3$ at room temperature (excitation at 242 nm), in which the peak representing the M···M interaction is designated by an asterisk (*) in the plot. ([#]Overtone of excitation at 242 nm).

https://doi.org/10.1021/acsomega.2c06729
ACS Omega 2023, 8, 6439−6454

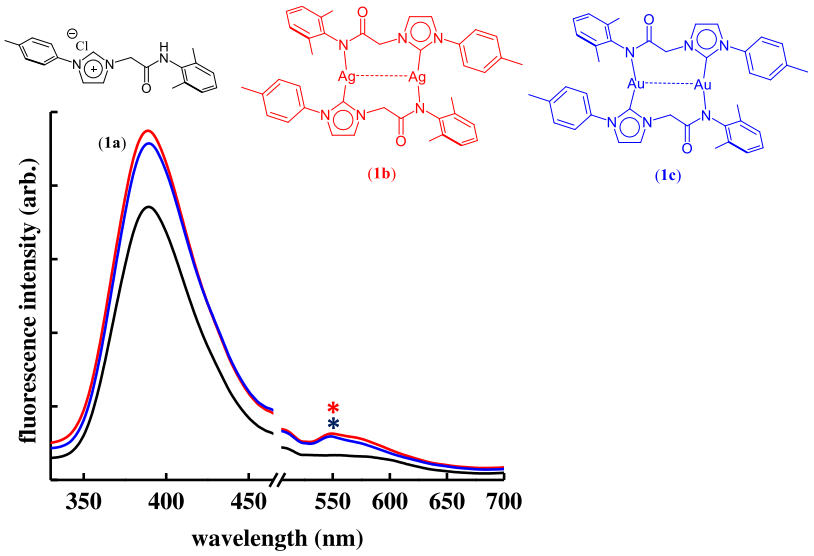

Figure 5. Comparison of the emission spectra (expanded) of the ligand (**1a**), the Ag−NHC complex (**1b**), and the Au−NHC complex (**1c**) in the solid state at room temperature (excitation at 242 nm), in which the peak representing the M···M interaction is designated by an asterisk (*) in the plot.

The absorption spectra of silver **1b**−**4b** and gold **1c**−**4c** complexes in $CHCl_3$ have been computed using the TD-DFT method to comprehend the electronic transition. The experimental and computed findings of λ_{abs}^{max} of different complexes using various functionals with various basis sets are given in Table S2. The B3LYP functional at LANL2DZ/6-31G(d) overestimates vertical excitation energies around 40 nm, while at the def2tzvp level about only 30 nm. The nonempirical PBE0 functional frequently used in benchmarks offers excellent results when compared to other density functionals, at least for the electronic vertical transitions.[36] We also tried this exchange−correlation functional, and expectedly, PBE0 results agreed with experimental excitation energies. Table S3 lists the predicted maximum absorption energies (wavelengths) along with their oscillator strengths, primary contributions from different electronic transitions, excited states, and assignments in addition to the available experimental findings. The frontier orbitals involved in these transitions for different complexes are given in Figure S97. Based on our TD-DFT frontier orbitals analysis, all of the complexes' bands may be described as an admixture of MLCT, LMCT, and ILCT states. We conducted the natural transition orbital (NTO) analysis based on the computed transition density matrices to examine the nature of absorption. Natural transition orbitals offer a more intuitive representation of the orbitals when excited states of molecules with highly delocalized chromophores or many chromophoric sites are involved. In terms of an expansion into single-particle transitions, this technique provides the most condensed depiction of the transition density between the ground and excited states. The terms "particle" and "hole" transition orbitals are used here to designate the vacant and occupied NTOs, respectively. The NTOs for all complexes are given in Figure S98. Based on our TD-DFT NTO analysis, all of the complexes' bands may be described as an admixture of MLCT, LMCT, and ILCT states. Optically excited transition orbitals move from occupied (hole) to unoccupied (electron) transition orbitals. Hole NTOs are delocalized on N−Ag−Ag−N (N−Au−Au−N), while particle NTOs are mainly delocalized on C−Ag−Ag−C (C−Au−Au−C). By frontier orbitals and NTO, we may conclude that the main contributor for the transition arises from $d_{x^2-y^2} - d_{x^2-y^2}$ (Ag/Au) − d_σ to π^* orbitals of the aromatic ring.

The semiempirical, Hartree−Fock, correlated methods like MP2 calculations suggest that the dispersion interaction is the dominant attractive component of metallophilic interactions and becomes more favorable when descending in group 11.[24] On the other hand, dispersion-corrected DFT calculations have suggested that dispersion contributions are substantially less important than MP2 computations and that they are also relatively independent of the metal.[24] Similarly, QCSID and CCSDT methods also contradict MP2 methods and support stronger argentophilic interactions compared to aurophilic interactions.[24] Recent energy decomposition analysis suggests a combination of electrostatic interactions and weakly covalent M···M orbital interactions, both of which are counterbalanced by Pauli repulsion, which dictate the strength of metallophilic interactions.[37] Based on this, we performed the atoms in molecules (AIM) analysis and constructed the topological diagrams for the silver **1b**−**4b** and the gold **1c**−**4c** complexes (Table 4 and Figure 6). The AIM analysis indicated the presence of a bond critical point (BCP) between two metal ions in all of the cases barring **2c**, suggesting favorable metallophilic interactions. The electron density $\rho(r)$, which measures the strength of this interaction, is found to be 0.019 au (**1b**), 0.0076 au (**2b**), 0.011 au (**3b**), 0.023 au (**4b**), 0.017 au (**1c**), 0.010 (**3c**) au, and 0.012 au (**4c**) (Table 4). The interaction energy,[38] $E_{int} = V/2$, at the M···M bond critical point is found to be −18.6 (**1b**), −4.5 (**2b**), −8.7 (**3b**), −25.7 (**4b**), −14.7 (**1c**), −7.5 (**3c**), and −8.8 (**4c**) (Table 4). The electron density $\rho(r)$ and interaction energy E_{int} values of **1b**−**4b** complexes are higher than those of **1c**−**4c**, which indicates that the argentophilic interactions in the silver **1b**−**4b** complexes are stronger. These values are smaller than the strong metallophilic interactions reported, like 0.042 au in a silver (*N*,*N*′-Di-*i*-propylacetamidinate) complex,[39] and suggest that the strength of interactions decreases in the following order: **4b** > **1b** > **1c** > **4c** > **3b** > **3c** > **2b**. A small value of the electron density, positive Laplacian value, and negative values of the total electronic energy density $H(r)$ at the BCP generally

https://doi.org/10.1021/acsomega.2c06729
ACS Omega 2023, 8, 6439−6454

Table 2. Comparison of the Crystallographic and Photoluminescence Data of the Large 12-Membered Metallamacrocyclic Ag−NHC Complexes 1b−4b with Those Known in the Literature

S. No.	complex	d[Ag(1)−C(1)]/ (Å)	d[Ag−N_{amido}]/ (Å)	d[Ag•••Ag]/ (Å)	∠ C(1)−Ag(1)−N(3) (°)	Ag•••Ag emission band/ (λ) nm		reference
						in $CHCl_3$	solid state	
1	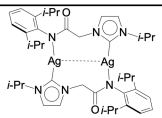	2.066(8)	2.084(6)	3.4026(8)	171.2(6)	647	635	[33]
2	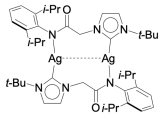	2.032(4), 2.045(4)	2.073(3) , 2.073(3)	3.7706(10)	170.31(14)	630	632	[33]
3	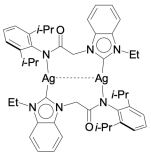	2.073(2)	2.0898(18)	3.1894(3)	168.61(8)	534	530	[32]
4	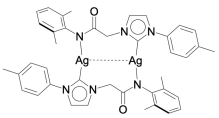 **(1b)**	2.071(2)	2.0971(16)	3.1061(3)	167.90(7)	534	549	this work
5	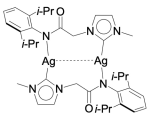 **(2b)**	2.0594(2)	2.0831(15)	3.6495(4)	170.01(6)	534	553	this work
6	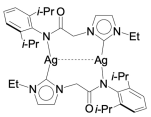 **(3b)**	2.0621(17)	2.0911(13)	3.3810(4)	166.36(6)	533	559	this work
7	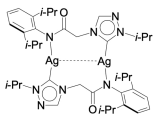 **(4b)**	2.054(8)	2.125(6)	2.9974(8)	176.1(3)	534	552	this work

suggest closed-shell electrostatic interactions.[40] Further, the $|V(r)|/G(r)$ ratio for complexes, except for **4b**, is close to unity, suggesting closed-shell interactions.[40] The order of this ratio is found to be **1b** > **1c** > **3b** > **4c** > **3c** > **2b** > **4b**, and the covalency contribution decreases in the same order.

Apart from AIM, we have also performed NCI analysis that is widely used to understand the nature of noncovalent interactions.[41,42] The divergence from a uniform electron distribution is explained by the dimensionless function known as the reduced density gradient (RDG). In regions far from the molecule where the density quickly decays to zero, the RDG will have very large positive values, and in regions with covalent bonds and noncovalent interactions, it will have very low values that are essentially negligible. RDG is a function of electron density and its gradient and is given by eq 1.[41]

$$s(\rho) = \frac{|\nabla\rho|}{2\sqrt{3\pi^2\rho^4}} \quad (1)$$

Although low gradient density regions enable the identification of weak interactions in a molecular system, it is unable to differentiate various contributions to the noncovalent interactions, such as attractive and repulsive interactions. For this purpose, the sign of $(\lambda_2)\rho$ (λ_2 is the largest eigen value of the Hessian matrix, $\lambda_2 < 0$ and $\lambda_2 > 0$ for bonding and nonbonding interactions, respectively) from noncovalent interaction (NCI) analysis can be utilized.[41] The noncovalent interaction (NCI) and reduced density gradient (RDG) scatter plots[42] for the silver **1b**−**4b** and the gold **1c**−**4c** complexes are shown in Figure 7. In the plots, the blue colored spikes in the negative region of the scatter plot correspond to the hydrogen bonds, the red colored spikes represent the strong repulsive interactions, and the green region indicates the van der Waals interaction. The metallophilic interaction region is circled in the NCI plot, and if we carefully analyze this region across the plot, the following points emerge: (i) for the **1b**, **1c**, and **4b** complexes, this region is dominated by blue color, which suggests a dominant attractive interaction in these complexes

https://doi.org/10.1021/acsomega.2c06729
ACS Omega 2023, 8, 6439−6454

Table 3. Comparison of the Crystallographic and Photoluminescence Data of the Large 12-Membered Metallamacrocyclic Au−NHC Complexes 1c−4c with Those Known in the Literature

S. No.	complex	d[Au(1)−C(1)]/ (Å)	d[Au−N_{amido}]/ (Å)	d[Au•••Au]/ (Å)	∠ C(1)−Au(1)−N(3) (°)	Au•••Au emission band/ (λ) nm		reference
						in $CHCl_3$	solid state	
1	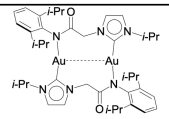	1.982(3)	2.037(3)	3.9854(4)	177.32(12)	623	630	[33]
2	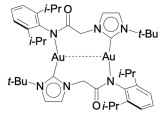	1.989(3), 1.990(3)	2.039(3) , 2.030(3)	3.8989(7)	172.86(13)	627	631	[33]
3	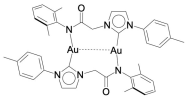 (1c)	1.993(2)	2.0457(17)	3.3462(2)	171.09(8)	532	548	this work
4	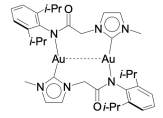 (2c)	1.996(3)	2.050(2)	4.2597(8)	176.91(10)	533	552	this work
5	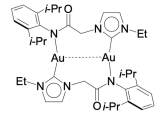 (3c)	1.985(4)	2.047(3)	3.6358(5)	170.64(13)	532	559	this work
6	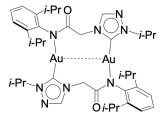 (4c)	1.975(4)	2.031(3)	3.7151(5) and 3.5640(5)	172.00(14)	530	552	this work

Table 4. Topological Parameters of Different Complexes at the M···M Bond Critical Point

parameter	1b	2b	3b	4b	1c	3c	4c
$\rho(r)$ (au)	0.0192	0.0076	0.0118	0.0234	0.0172	0.0104	0.0119
$G(r)$ (au)	0.0129	0.0037	0.0067	0.0172	0.0106	0.0059	0.0069
$K(r)$ (au)	0.0012	−0.0003	−0.0001	0.0023	0.0005	−0.0002	−0.0001
$V(r)$ (au)	−0.0142	−0.0034	−0.0066	−0.0196	−0.0112	−0.0057	−0.0067
$H(r)$ (au)	−0.0012	0.0003	0.0001	−0.0023	−0.0005	0.0002	0.0001
$\nabla^2\rho(r)$ (au)	0.0467	0.01621	0.0275	0.0596	0.0407	0.0250	0.0283
H/ρ	−0.0653	0.0417	0.0082	−0.010	−0.0297	0.0255	0.0124
$\lvert V\rvert/G$	1.100	0.9155	0.986	0.137	1.05	0.955	0.979
$E_{int} = V/2$ (kJ/mol)	−18.6	−4.5	−8.7	−25.7	−14.7	−7.5	−8.8

and (ii) for the remaining **2b**, **3b**, **2c**, **3c**, and **4c** complexes, the green color is dominant, and this suggests that the interaction has a dominant van der Waals contribution. Complementary to the NCI plot regions, we can see the corresponding spikes in the scatter plots in the negative region for **1b**, **1c**, and **4b**, which are blue in color, whereas for the **2b**, **3b**, **2c**, **3c**, and **4c** complexes, the spikes are dominantly green reaffirming our point.

The NBO analysis performed yields natural population analysis (NPA) on different atoms that offers further insights into metal−metal interactions (Table S4). The charges on silver atoms are more compared to that of gold atoms in all complexes. The charges on pairs of atoms (Ag1, $Ag1^i$) or (Au1, $Au1^i$), (N3, $N3^i$), and (C1, $C1^i$) are almost similar except in the case of **4b** and **4c**. A significant positive charge on Ag1 or Au1 and a concomitant negative charge on the N3 atom in **2b** or **2c** leads to a larger Ag···Ag or Au···Au distance. In **4b** and **4c**, on the other hand, a significant less negative charge on N1 and a no charge on C attached to N1 are found, and this is found to strengthen the Ag···Ag or Au···Au interaction. In the **2b**, **3b**, and **4b** complexes, the groups attached to N1/$N1^i$ are methyl, ethyl, and *i*-propyl, respectively; however, the groups attached to N3/$N3^i$ are constant. The steric hindrance capacity normally increases from methyl to *i*-propyl groups. The negative charge on the carbon atom is found to increase from *i*-propyl to methyl groups. The charges on N1 and $N1^i$

https://doi.org/10.1021/acsomega.2c06729
ACS Omega 2023, 8, 6439−6454

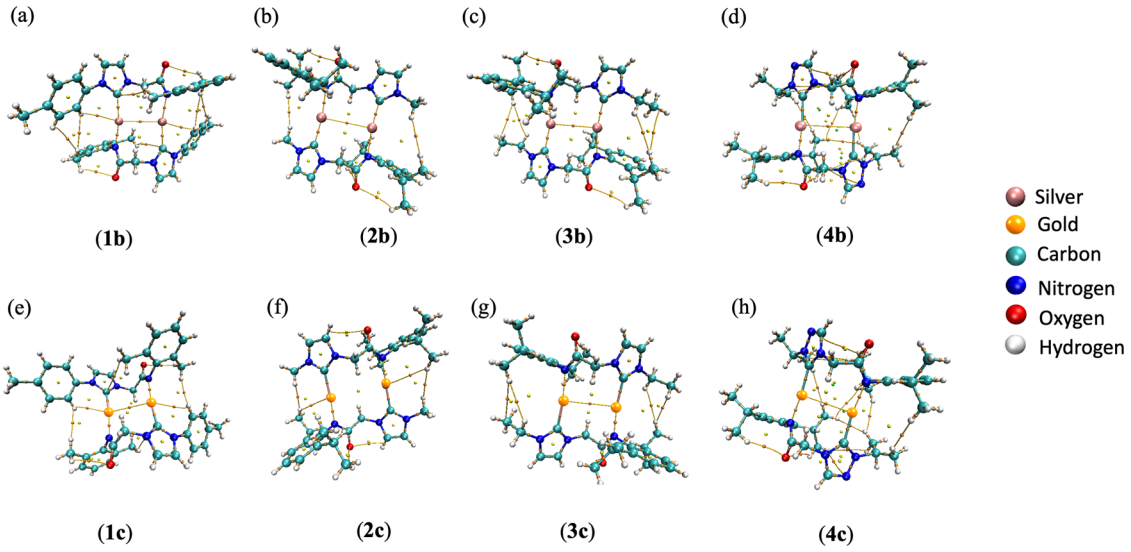

Figure 6. AIM computed topological diagrams for different complexes (a) **1b**, (b) **2b**, (c) **3b**, (d) **4b**, (e) **1c**, (f) **2c**, (g) **3c**, and (h) **4c**. (Color code: yellow, ring critical point and green, cage critical point).

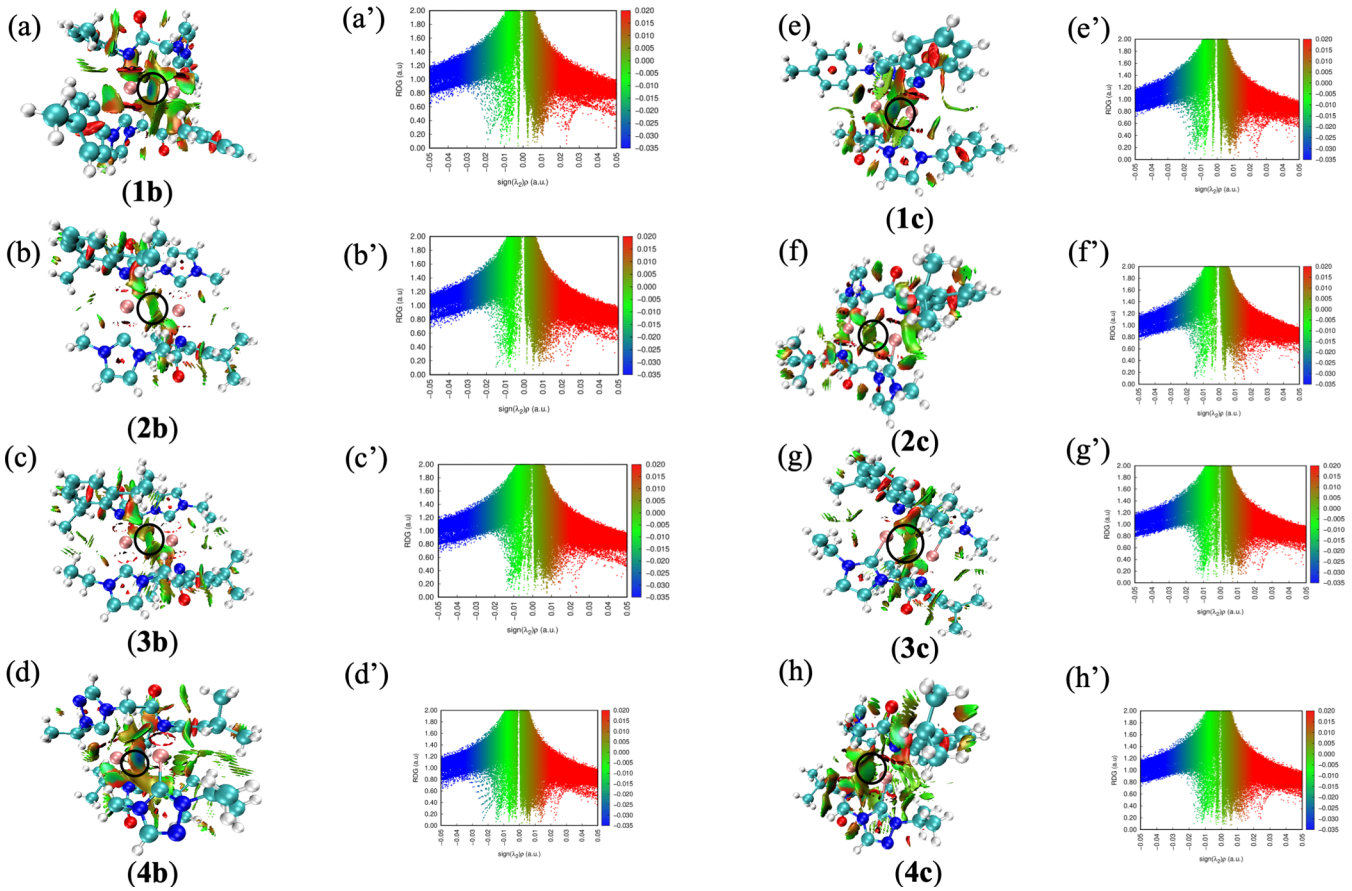

Figure 7. NCI plots of complexes (a) **1b**, (b) **2b**, (c) **3b**, (d) **4b**, (e) **1c**, (f) **2c**, (g) **3c**, and (h) **4c** and RDG scatter plots of complexes (a′) **1b**, (b′) **2b**, (c′) **3b**, (d′) **4b**, (e′) **1c**, (f′) **2c**, (g′) **3c**, and (h′) **4c**.

Table 5. Wiberg Bond Indices of Selected Bonds for Silver 1b−4b and Gold 1c−4c Complexes

bonds	1b	2b	3b	4b	1c	2c	3c	4c
Ag1−Ag1^{i} (Au1−Au1^{i})	0.16	0.09	0.13	0.17	0.17	0.04	0.12	0.13
Ag1−N3 (Au1−N3)	0.28	0.29	0.27	0.26	0.38	0.39	0.38	0.39
Ag1−C1 (Au1−C1)	0.47	0.50	0.49	0.45	0.65	0.67	0.67	0.66

https://doi.org/10.1021/acsomega.2c06729
ACS Omega 2023, 8, 6439−6454

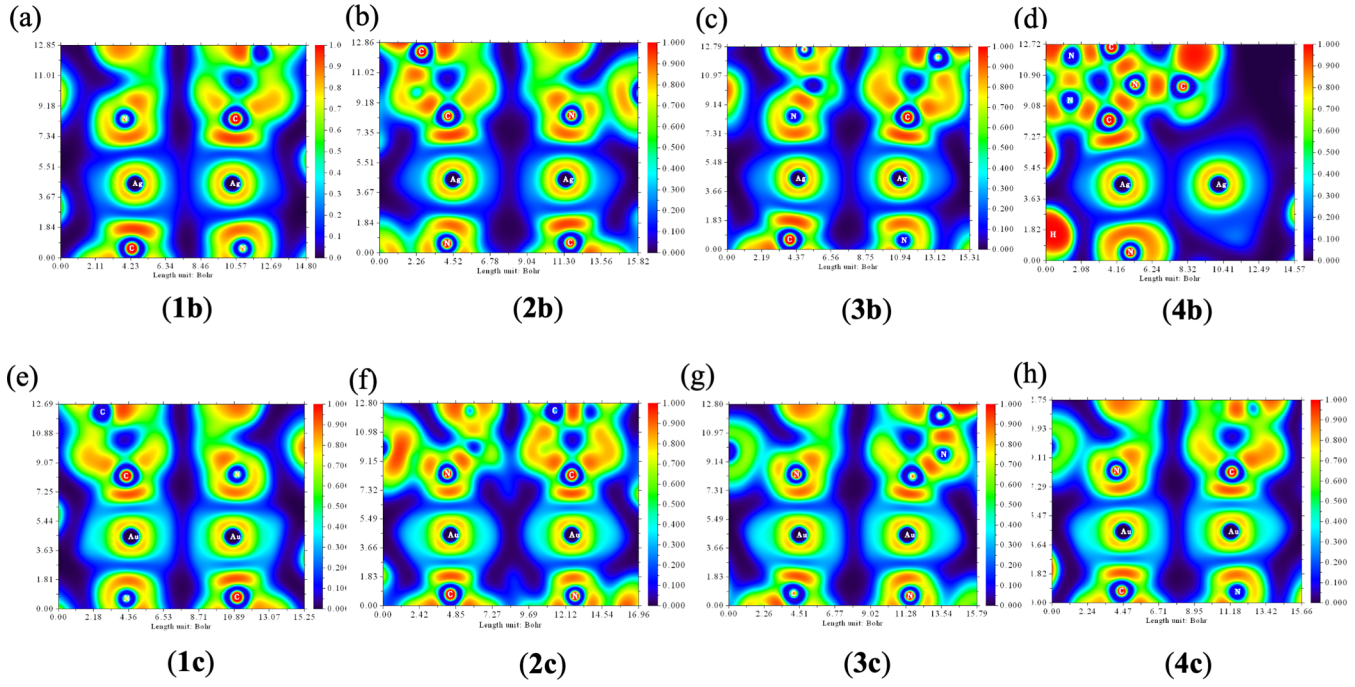

Figure 8. Electron localization function (ELF) color-filled maps of complexes (a) **1b**, (b) **2b**, (c) **3b**, (d) **4b**, (e) **1c**, (f) **2c**, (g) **3c**, and (h) **4c**.

are almost similar. The Wiberg bond index (WBI) (Table 5) is consistent with the metal···metal distance observed in the X-ray structure, with the shortest distance geometry (**4b**) yielding the largest WBI of 0.17. The WBI is found to be 0.16 (**1b**), 0.09 (**2b**), 0.13 (**3b**), 0.17 (**4b**), 0.17 (**1c**), 0.04 (**2c**), 0.12 (**3c**), and 0.13 (**4c**) (Table 5). This again indicates that argentophilic interactions in **2b**−**4b** is stronger than aurophilic interactions in **2c**−**4c**, with **1b** and **1c** being nearly equal. Further, we observe that the Ag1−N3 and the Ag1−C1 bond's WBI values are inversely proportional to the Ag···Ag interaction, and the same trend is observed for the WBI values for Au1−N3 and the Au1−C1 bonds in the case of the Au···Au interaction. The stronger argentophilic interactions compared to aurophilic interactions may be attributed to stronger Pauli repulsion between Au···Au centers.[25,43] In short, the electronic and the steric factors of the group attached to N1 significanlty influences the M···M interactions.

Further electron localization function (ELF) analyses were performed to probe the localization of electron density corresponding to the M···M interactions (Figure 8). The electron localization function (ELF) is a simple measure of electron localization in an atomic and molecular system. The ELF is defined by eq 2[44]

$$\mathrm{ELF}(\mathbf{r}) = \frac{1}{1 + [\frac{D(\mathbf{r})}{D_0(\mathbf{r})}]^2} \tag{2}$$

where

$$D(\mathbf{r}) = \frac{1}{2}\sum_i \eta_i |\nabla\varphi_i(\mathbf{r})|^2 - \frac{1}{8}\frac{|\nabla\rho(\mathbf{r})|^2}{\rho(\mathbf{r})} \tag{3}$$

$$D_0(\mathbf{r}) = (3/10)(3\pi^2)^{2/3}\rho(\mathbf{r})^{5/3} \tag{4}$$

$D(\mathbf{r})$ is defined as the difference between the kinetic energy density and the bosonic kinetic energy density, $D_0(\mathbf{r})$ is taken as a reference (uniform electron gas), and ρ is the electron charge density.

The ELF is a relative measurement of the electron localization, and therefore, the ELF values are expected to be in the range of 0 to 1. In general, in the bonding regions, the ELF($\mathbf{r}$) is expected to reach unity,[45] and when ELF($\mathbf{r}$) is greater than 0.7, electrons are characterized as localized (core or bonding regions or lone pairs). On the other hand, when the value of ELF is less than 0.7, the electron localization is similar to that of an electron−gas, which is typical of metallic bonds.[46]

Similar to ELF, Schmider and Becke defined another function for finding high localization zones called the localized orbital locator (LOL). The LOL is given by eq 5.[47]

$$\mathrm{LOL}(\mathbf{r}) = \frac{\tau(\mathbf{r})}{1 + \tau(\mathbf{r})} \tag{5}$$

where

$$\tau(\mathbf{r}) = \frac{D_0(\mathbf{r})}{\left(\frac{1}{2}\right)\sum_i \eta_i |\nabla\varphi_i(\mathbf{r})|^2} \tag{6}$$

$D_0(\mathbf{r})$ is defined similar to ELF. Generally speaking, LOL and ELF are qualitatively comparable, but LOL communicates a more distinct and decisive picture than ELF.[48]

The ELF values computed at the M···M bond critical point were found to be 0.085 (**1b**), 0.047 (**2b**), 0.063 (**3b**), 0.091 (**4b**), 0.088 (**1c**), 0.055 (**3c**), and 0.062 (**4c**) (the ELF value for **2c** is negligible). Further, the LOL values computed at the M···M bond critical point were found to be 0.234 (**1b**), 0.183 (**2b**), 0.206 (**3b**), 0.241 (**4b**), 0.236 (**1c**), 0.194 (**3c**), and 0.204 (**4c**). The difference between ELF and LOL values is in the range of 0.12−0.15. The ELF and LOL values are small, indicating only weak metallophilic interactions, and this ELF and LOL order also supports the strengths of the M···M interaction. The ELF and LOL values at the M···M bond critical point of **2b**−**4b** complexes are higher than those of **2c**−**4c** (**1b** and **1c** nearly the same), which indicates that at least the argentophilic interactions in the silver **2b**−**4b** complexes

https://doi.org/10.1021/acsomega.2c06729
ACS Omega 2023, 8, 6439−6454

are stronger, which again suggests that the argentophilic interactions in the silver **2b**−**4b** complexes are stronger. In conclusion, ELF and LOL values, WBI indices, electron density ($\rho(r)$), interaction energy (E_{int}), crystallographic study, and photoluminescence spectra studies suggest that argentophilic interactions are most likely stronger than the aurophilic interactions in these complexes.

CONCLUSIONS

In summary, a series of four pairs of new large 12-membered silver **1b**−**4b** and gold **1c**−**4c** metallamacrocycles of amido-functionalized imidazole and 1,2,4-triazole-derived N-heterocyclic carbenes, displaying discrete singular metallophilic interactions, as corroborated by the single-crystal X-ray diffraction and the photoluminescence studies, have been synthesized. Furthermore, the computational studies indicate that the N-heterocyclic carbene-based ligand architecture led to strong metallophilic interactions in these complexes. The strength of the M···M interactions, as determined from the electron density at the bond critical point (BCP) from topological analysis and the Wiberg bond index (WBI) from the natural bond orbital (NBO) analysis, suggested that the metallophilic interaction decreased in the order **4b** > **1b** > **1c** > **4c** > **3b** > **3c** > **2b** > **2c**. The metallophilic interactions were visualized using scatter plots and NCI plots and were quantified using ELF functions. The steric factors at the N1-position and the charge of carbon attached to the N1-position influences the metallophilic interactions. In conclusion, both steric effects and the electronic effects of the N-heterocyclic carbene control the metallophilic interactions. ELF and LOL values, WBI indices, electron density ($\rho(r)$), interaction energy (E_{int}), crystallographic study, and photoluminescence spectra studies suggest that argentophilic interactions in **1b**−**4b** complexes are stronger than the aurophilic interactions in the **1c**−**4c** complexes.

EXPERIMENTAL SECTION

All manipulations were carried out using a combination of a glovebox and standard Schlenk techniques. Solvents were purified and degassed by standard procedures. 1-(4-Methylphenyl)imidazole,[49] 1-ethylimidazole,[50] 1-*i*-propyltriazole,[51] 2-chloro-*N*-(2,6-di-methylphenyl)acetamide,[52] 2-chloro-*N*-(2,6-di-i-propylphenyl)acetamide,[52] and (SMe_2)-AuCl[53] were synthesized by the modified literature procedures. ^{1}H and ^{13}C{^{1}H} NMR spectra were recorded on Varian and Bruker 400 MHz and Bruker 500 MHz NMR spectrometers. ^{1}H NMR peaks are labeled as singlet (s), doublet (d), triplet (t), doublet of doublets (dd), multiplet (m), and septet (sept). Infrared spectra were recorded on a PerkinElmer Spectrum One FT-IR spectrometer. Mass spectrometry measurements were done on a Micromass Q-Tof and Bruker Maxis Impact spectrometer. Elemental analysis was carried out on a Thermo Quest FLASH 1112 SERIES (CHNS) elemental analyzer. The crystals for the compound **1b**−**4b** and **1c**−**4c** were grown in CH_3CN by a slow evaporation technique. Single-crystal X-ray diffraction studies were performed on a Rigaku Hg724+ diffractometer for compounds **1b**−**4b** and on Bruker D8 Quest diffractometer for compounds **1c**−**4c**, and crystal data collection and refinement parameters are summarized in Table S1. The structures were solved using SHELXT and refined via the full matrix least-squares method with SHELXL-2018/3, refining on F^2.[54] The CCDC − 1876407 (for **1b**), 2170371 (for **1c**), 1876404 (for **2b**), 2173119 (for **2c**), 1882493 (for **3b**), 2160247 (for **3c**), 1887221 (for **4b**), and 2177632 (for **4c**) contain supplementary crystallographic data for this paper. These data can be obtained from the Cambridge Crystallographic Data Centre via www.ccdc.com.ac.uk/datarequest/cif.

Synthesis of 1-(4-Me-Phenyl)-3-*N*-(2,6-Me_2-phenylacetamido)-imidazolium Chloride (1a). 1-(4-Me-Phenyl)-imidazole (2.00 g, 12.7 mmol) and 2-chloro-*N*-(2,6-Me_2-phenyl)acetamide (2.76 g, 14.0 mmol) were refluxed in toluene (ca. 25 mL) for 12 h, after which the reaction mixture was cooled to 30 °C. The formed solid was filtered off and washed repeatedly with diethyl ether to give the crude product, which was purified by column chromatography on neutral silica using $CHCl_3$/CH_3OH (9.5:0.5 v/v) mixed medium to give the product (**1a**) as a light brown solid (1.86 g, 41%). ^{1}H NMR ($CDCl_3$, 500 MHz, 25 °C): δ, 10.48 (s, 1H, NC*H*N), 10.1 (s, 1H, N*H*), 7.81 (s, 1H, NC*H*CHN), 7.42 (s, 1H, NCHC*H*N), 7.35 (d, 2H, $^3J_{HH}$ = 8 Hz, 4-(CH_3)C_6H_4), 7.18 (d, 2H, $^3J_{HH}$ = 8 Hz, 4-(CH_3)C_6H_4), 6.9 (t, 1H, $^3J_{HH}$ = 6 Hz, 2,6-(CH_3)$_2C_6H_3$), 6.84 (d, 2H, $^3J_{HH}$ = 7 Hz, 2,6-(CH_3)$_2C_6H_3$), 5.71 (s, 2H, CH_2), 2.29 (s, 3H, 4-(CH_3)C_6H_4), 2.10 (s, 6H, 2,6-(CH_3)$_2C_6H_3$). ^{13}C{^{1}H} NMR ($CDCl_3$, 125 MHz, 25 °C): δ ppm, 163.6 (*C*O), 140.7 (4-(CH_3)*C*$_6H_4$), 135.9 (N*C*HN), 135.3 (2,6-(CH_3)$_2$*C*$_6H_3$), 133.6 (4-(CH_3)*C*$_6H_4$), 132 (2,6-(CH_3)$_2$*C*$_6H_3$), 130.9 (4-(CH_3)*C*$_6H_4$), 127.9 (2,6-(CH_3)$_2$*C*$_6H_3$), 127.1 (2,6-(CH_3)$_2$*C*$_6H_3$), 124.6 (N*C*HCHN), 121.6 (4-(CH_3)*C*$_6H_4$), 120.2 (NCH*C*HN), 51.9 (*C*H_2), 21.1 (4-(*C*H_3)C_6H_4), 18.7 (2,6-(*C*H_3)$_2C_6H_3$). IR data (cm^{-1}) KBr pellet: 3406 (m), 3253 (m), 3049 (m), 1671 (s), 1547 (s), 1471 (m), 1441 (w), 1267 (w), 1239 (m), 1073 (w), 819 (w), 763 (w), 514 (w). HRMS (ESI): Calcd. for $[M - Cl]^+$, $[C_{20}H_{22}N_3O]^+$ m/z 320.1757; found m/z 320.1755. Anal. Calcd. for $C_{20}H_{22}N_3OCl$: C, 67.50; H, 6.23; N, 11.81; Found: C, 67.20; H, 6.413; N, 11.57%.

Synthesis of [1-(4-Me-Phenyl)-3-*N*-(2,6-Me_2-phenylacetamido)-imidazol-2-ylidene]$_2Ag_2$ (1b). A solution of 1-(4-Me-phenyl)-3-(2,6-Me_2-phenyl)acetamido-imidazolium chloride (**1a**) (0.905 g, 2.54 mmol) in CH_2Cl_2 (ca. 50 mL) was stirred with Ag_2O (0.592 g, 2.55 mmol) in the dark at room temperature overnight. The reaction mixture was filtered over a pad of celite, and the solvent was evaporated. The residue was purified by column chromatography on neutral Al_2O_3 using the $CHCl_3$/CH_3OH (9.5:0.5) system to give the desired product (**1b**) as a grayish-white solid (0.551 g, 51%). ^{1}H NMR ($CDCl_3$, 500 MHz, 25 °C): δ ppm, 7.62 (s, 1H, NC*H*CHN), 7.16 (s, 1H, NCHC*H*N), 7.07 (d, 2H, $^3J_{HH}$ = 8 Hz, 4-(CH_3)C_6H_4), 6.99 (d, 2H, $^3J_{HH}$ = 8 Hz, 4-(CH_3)C_6H_4), 6.94 (d, 2H, $^3J_{HH}$ = 7 Hz, 2,6-(CH_3)$_2C_6H_3$), 6.90 (t, 1H, $^3J_{HH}$ = 7 Hz, 2,6-(CH_3)$_2C_6H_3$), 5.01 (s, 2H, CH_2), 2.37 (s, 3H, 4-(CH_3)C_6H_4), 1.90 (s, 6H, 2,6-(CH_3)$_2C_6H_3$). ^{13}C{^{1}H} NMR ($CDCl_3$, 125 MHz, 25 °C): δ ppm 176.9 (d, ^1J ^{109}Ag−$^{13}C_{carbene}$ = 251 Hz, ^1J ^{107}Ag−$^{13}C_{carbene}$ = 216 Hz, Ag−N*C*N), 168.1 (*C*O), 146.2 (2,6-(CH_3)$_2$*C*$_6H_3$), 138.8 (4-(CH_3)*C*$_6H_4$), 137.3 (4-(CH_3)*C*$_6H_4$), 132.1 (2,6-(CH_3)$_2$*C*$_6H_3$), 130.3 (4-(CH_3)*C*$_6H_4$), 127.8 (2,6-(CH_3)$_2$*C*$_6H_3$), 123.6 (2,6-(CH_3)$_2$*C*$_6H_3$), 123.5, (4-(CH_3)*C*$_6H_4$), 123.2 (N*C*HCHN), 121.5 (NCH*C*HN), 61.8 (*C*H_2), 21.0 (4-(*C*H_3)C_6H_4), 18.5 (2,6-(*C*H_3)$_2C_6H_3$). IR data (cm^{-1}) KBr pellet: 3452 (m), 3165 (m), 2938 (m), 1686 (m), 1601 (s), 1579 (s), 1515 (s), 1467 (m), 1438 (m), 1271 (m), 1238 (m), 1093 (w), 818 (m), 767 (m), 541 (w). Anal. Calcd. for $C_{40}H_{40}N_6O_2Ag_2$: C, 56.35; H, 4.73; N, 9.86; Found: C, 56.19; H, 4.797; N, 9.83%.

https://doi.org/10.1021/acsomega.2c06729
ACS Omega 2023, 8, 6439−6454

Synthesis of [1-(4-Me-Phenyl)-3-*N*-(2,6-Me$_2$-phenylacetamido)-imidazol-2-ylidene]$_2$Au$_2$ (1c). [1-(4-Me-Phenyl)-3-*N*-(2,6-Me$_2$-phenylacetamido)-imidazol-2-ylidene]$_2$Ag$_2$ (**1b**) (0.107 g, 0.127 mmol) and (SMe$_2$)AuCl (0.076 g, 0.260 mmol) were mixed in CH_2Cl_2 and stirred for 6 h at room temperature. An off-white AgCl solid precipitated out during the course of reaction, after which it was filtered. The filtrate was dried under vacuum to give the crude product, which was purified by column chromatography on neutral Al_2O_3 using a mixed medium of CH_2Cl_2/CH_3OH (9.5:0.5, v/v) to give the product as a white-colored solid (**1c**) (0.042 g, 32%). ^{1}H NMR ($CDCl_3$, 400 MHz, 25 °C): δ ppm, 7.58 (d, 1H, $^3J_{HH}$ = 2 Hz, NC*H*CHN), 7.22 (d, 2H, $^3J_{HH}$ = 8 Hz, 4-(CH_3)C_6H_4), 7.11 (d, 1H, $^3J_{HH}$ = 2 Hz, NCHC*H*N), 7.10−7.08 (m, 1H, 2,6-(CH_3)$_2C_6H_3$), 6.99 (d, 2H, $^3J_{HH}$ = 8 Hz, 4-(CH_3)C_6H_4), 6.96−6.95 (m, 2H, 2,6-(CH_3)$_2C_6H_3$), 5.34 (s, 2H, CH_2), 2.37 (s, 3H, 4-(CH_3)C_6H_4), 2.00 (s, 6H, 2,6-(CH_3)$_2C_6H_3$). ^{13}C{^{1}H} NMR ($CDCl_3$, 125 MHz, 25 °C): δ ppm 169.2 (N*C*N), 168.9 (*C*O), 144.7 (2,6-(CH_3)$_2$*C*$_6H_3$), 138.7 (4-(CH_3)*C*$_6H_4$), 136.6 (4-(CH_3)*C*$_6H_4$), 133.1 (2,6-(CH_3)$_2$*C*$_6H_3$), 129.8 (4-(CH_3)*C*$_6H_4$), 127.6 (2,6-(CH_3)$_2$*C*$_6H_3$), 124.4 (2,6-(CH_3)$_2$*C*$_6H_3$), 124.3, (4-(CH_3)*C*$_6H_4$), 122.9 (N*C*HCHN), 121.0 (NCH*C*HN), 58.8 (*C*H$_2$), 21.0 (4-(*C*H$_3$)C_6H_4), 18.2 (2,6-(*C*H$_3$)$_2C_6H_3$). IR data (cm^{-1}) KBr pellet: 3417 (br), 3117 (w), 2919 (m), 2356 (m), 1615 (s), 1516 (s), 1418 (w), 1099 (m), 765 (w). 679 (w). HRMS (ESI): Calcd. for [M + H]$^+$, [$C_{40}H_{41}N_6O_2Au_2$]$^+$ *m*/*z* 1031.2617; found *m*/*z* 1031.2615. Anal. Calcd. for $C_{40}H_{40}N_6O_2Au_2$: C, 46.61; H, 3.91; N, 8.15; Found: C, 46.43; H, 4.076; N, 8.18%.

Synthesis of 1-(Methyl)-3-*N*-(2,6-di-*i*-propylphenylacetamido)-imidazolium Chloride (2a). 1-Methyl imidazole (0.510 g, 6.21 mmol) and 2-chloro-N-(2,6-di-*i*-propylphenyl)-acetamide (1.58 g, 7.02 mmol) were refluxed overnight in toluene (ca. 50 mL), after which the reaction mixture was cooled to room temperature. The solvent was evaporated, and the remaining solid was washed repeatedly with diethyl ether to give the white solid, which was purified by column chromatography on neutral silica using the $CHCl_3$/CH_3OH (9.5:0.5) system to give the desired product (**2a**) as a white solid (1.04 g, 50%). ^{1}H NMR (DMSO-d_6, 400 MHz, 25 °C): δ ppm, 10.48 (s, 1H, NC*H*N), 9.24 (s, 1H, N*H*), 7.70 (s, 1H, NC*H*CHN), 7.67 (s, 1H, NC*H*CHN), 7.14 (t, 1H, $^3J_{HH}$ = 8 Hz, 2,6-($CH(CH_3)_2$)$_2$-C_6H_3), 7.03 (d, 2H, $^3J_{HH}$ = 8 Hz, 2,6-($CH(CH_3)_2$)$_2$-C_6H_3), 5.32 (s, 2H, CH_2), 3.79 (s, 3H, NCH_3), 2.98 (sept, 2H, $^3J_{HH}$ = 7 Hz, 2,6-(C*H*(CH_3)$_2$)$_2$-C_6H_3), 1.02 (br, 6H, 2,6-(CH(C*H*$_3$)$_2$)$_2$-C_6H_3), 0.96 (br, 6H, 2,6-(CH-(C*H*$_3$)$_2$)$_2$-C_6H_3). ^{13}C{^{1}H} NMR (DMSO-d_6, 100 MHz, 25 °C): δ ppm, 165.3 (*C*O), 146.4 (2,6-($CH(CH_3)_2$)$_2$-*C*$_6H_3$), 138.2 (N*C*HN), 132.1 (2,6-($CH(CH_3)_2$)$_2$-*C*$_6H_3$), 128.2 (2,6-($CH(CH_3)_2$)$_2$-*C*$_6H_3$), 123.9 (N*C*HCHN), 123.7 (NCH*C*HN), 123.4 (2,6-($CH(CH_3)_2$)$_2$-*C*$_6H_3$), 51.1 (*C*H$_2$), 36.3 (N*C*H$_3$), 28.4 (2,6-(*C*H(CH_3)$_2$)$_2$-C_6H_3), 24.4 (2,6-(CH(*C*H$_3$)$_2$)$_2$-C_6H_3), 23.7 (2,6-(CH(*C*H$_3$)$_2$)$_2$-C_6H_3). IR data (cm^{-1}) KBr pellet: 3445 (m), 3145 (m), 3051 (m), 2964 (s), 2861 (m), 1696 (s), 1540 (m), 1461 (w), 1266 (w), 1176 (m), 954 (w), 800 (w), 628 (w). HRMS (ESI): Calcd. for [M − Cl]$^+$, [$C_{18}H_{26}N_3O$]$^+$ *m*/*z* 300.2070; found *m*/*z* 300.2076. Anal. Calcd. for $C_{18}H_{26}N_3OCl$: C, 64.37; H, 7.80; N, 12.51; Found: C, 64.05; H, 7.634; N, 12.39%.

Synthesis of [1-(Methyl)-3-*N*-(2,6-di-*i*-propylphenylacetamido)-imidazol-2-ylidene]$_2$Ag$_2$ (2b). A solution of 1-(methyl)-3-*N*-(2,6-di-*i*-propylphenyl)acetamido-imidazolium chloride (**2a**) (0.504g, 1.50 mmol) in CH_2Cl_2 (*ca.* 50 mL) was stirred with Ag_2O (0.358 g, 1.54 mmol) in the dark at room temperature overnight. The solvent was evaporated, and the residue was purified by column chromatography on neutral Al_2O_3 using the $CHCl_3$/CH_3OH (9.5:0.5) system to give the desired product (**2b**) as a grayish-white solid (0.152 g, 25%). ^{1}H NMR ($CDCl_3$, 500 MHz, 25 °C): δ ppm, 7.31 (s, 1H, NC*H*CHN), 7.18 (t, 1H, $^3J_{HH}$ = 9 Hz, 2,6-($CH(CH_3)_2$)$_2$-C_6H_3), 7.05 (d, 2H, $^3J_{HH}$ = 9 Hz, 2,6-($CH(CH_3)_2$)$_2$-C_6H_3), 6.92 (s, 1H, NCHC*H*N), 5.31 (s, 2H, CH_2), 3.79 (s, 3H, NCH_3), 3.03 (sept, 2H, $^3J_{HH}$ = 8 Hz, 2,6-(C*H*(CH_3)$_2$)$_2$-C_6H_3), 1.02 (d, 12H, $^3J_{HH}$ = 8 Hz, 2,6-(CH(C*H*$_3$)$_2$)$_2$-C_6H_3). ^{13}C{^{1}H} NMR ($CDCl_3$, 125 MHz, 25 °C): δ ppm, 182.3 (Ag−N*C*N), 166.8 (*C*O), 146.1 (2,6-($CH(CH_3)_2$)$_2$-*C*$_6H_3$), 131.2 (2,6-($CH(CH_3)_2$)$_2$-*C*$_6H_3$), 128.0 (2,6-($CH(CH_3)_2$)$_2$-*C*$_6H_3$), 123.2 (N*C*HCHN), 123.1 (2,6-($CH(CH_3)_2$)$_2$-*C*$_6H_3$), 121.7 (NCH*C*HN), 53.9 (*C*H$_2$), 38.7 (N*C*H$_3$), 28.6 (2,6-(*C*H-(CH_3)$_2$)$_2$-C_6H_3), 23.7 (2,6-(CH(*C*H$_3$)$_2$)$_2$-C_6H_3). IR data (cm^{-1}) KBr pellet: 3442 (w), 3163 (w), 2957 (s), 2866 (m), 1694 (m), 1529 (s), 1460 (m), 1266 (w), 798 (w), 743 (m). Anal. Calcd. for $C_{36}H_{48}N_6O_2Ag_2$: C, 53.21; H, 5.95; N, 10.34; Found: C, 53.40; H, 6.373; N, 10.34%.

Synthesis of [1-(Methyl)-3-*N*-(2,6-di-*i*-propylphenylacetamido)-imidazol-2-ylidene]$_2$Au$_2$ (2c). [1-(Methyl)-3-N-(2,6-di-*i*-propylphenylacetamido)-imidazol-2-ylidene]$_2$Ag$_2$ (**2b**) (0.124 g, 0.153 mmol) and (SMe$_2$)AuCl (0.090 g, 0.307 mmol) were mixed in CH_2Cl_2 and stirred for 6 h at room temperature. An off-white AgCl solid precipitated out during the course of reaction, after which it was filtered. The filtrate was dried under vacuum to give the crude product, which was purified by column chromatography on neutral Al_2O_3 using a mixed medium of CH_2Cl_2/CH_3OH (9.5:0.5, v/v) to give the product as a white-colored solid (**2c**) (0.041 g, 27%). ^{1}H NMR ($CDCl_3$, 400 MHz, 25 °C): δ ppm, 7.30 (t, 1H, $^3J_{HH}$ = 8 Hz, 2,6-($CH(CH_3)_2$)$_2$-C_6H_3), 7.25 (d, 1H, $^3J_{HH}$ = 2 Hz, NCHC*H*N), 7.16 (d, 2H, $^3J_{HH}$ = 8 Hz, 2,6-($CH(CH_3)_2$)$_2$-C_6H_3), 7.00 (d, 1H, $^3J_{HH}$ = 2 Hz, NCHC*H*N), 5.07 (s, 2H, CH_2), 3.87 (s, 3H, NCH_3), 3.03 (sept, 2H, $^3J_{HH}$ = 7 Hz, 2,6-(C*H*(CH_3)$_2$)$_2$-C_6H_3), 1.16 (d, 12H, $^3J_{HH}$ = 7 Hz, 2,6-(CH(C*H*$_3$)$_2$)$_2$-C_6H_3). ^{13}C{^{1}H} NMR ($CDCl_3$, 100 MHz, 25 °C): δ ppm, 172.1 (N*C*N), 165.3 (*C*O), 146.2 (2,6-($CH(CH_3)_2$)$_2$-*C*$_6H_3$), 129.8 (2,6-($CH(CH_3)_2$)$_2$-*C*$_6H_3$), 128.8 (2,6-($CH(CH_3)_2$)$_2$-*C*$_6H_3$), 123.5 (2,6-($CH(CH_3)_2$)$_2$-*C*$_6H_3$), 122.2 (N*C*HCHN), 122.1 (NCH*C*HN), 54.0 (*C*H$_2$), 38.4 (N*C*H$_3$), 28.9 (2,6-(*C*H(CH_3)$_2$)$_2$-C_6H_3), 23.7 (2,6-(CH-(*C*H$_3$)$_2$)$_2$-C_6H_3). IR data (cm^{-1}) KBr pellet: 3454 (s), 2964 (s), 2866 (m), 1666 (s), 1530 (m), 1467 (m), 1237 (w), 791 (w), 739 (m). HRMS (ESI): Calcd. for [M + Na]$^+$, [$C_{36}H_{48}N_6O_2Au_2Na$]$^+$ *m*/*z* 1013.3062; found *m*/*z* 1013.3067. Anal. Calcd. for $C_{36}H_{48}N_6O_2Au_2$: C, 43.64; H, 4.88; N, 8.48; Found: C, 43.30; H, 4.768; N, 8.55%.

Synthesis of 1-(Ethyl)-3-*N*-(2,6-di-*i*-propylphenylacetamido)-imidazolium Chloride (3a). 1-Ethylimidazole (1.00 g, 10.49 mmol) and 2-chloro-*N*-(2,6-di-*i*-propylphenyl)-acetamide (2.66 g, 10.49 mmol) were refluxed overnight in toluene (ca. 25 mL), after which the reaction mixture was cooled to 30 °C. The formed solid was filtered off and washed repeatedly with Et_2O to give the crude product, which was purified by column chromatography on neutral alumina using $CHCl_3$/CH_3OH (9.5:0.5 v/v) mixed medium to give the product (**3a**) as a white solid (1.28 g, 35%). ^{1}H NMR ($CDCl_3$, 500 MHz, 25 °C): δ ppm, 10.53 (s, 1H, NC*H*N), 9.84 (s, 1H, N*H*), 7.69 (s, 1H, NC*H*CHN), 7.29 (s, 1H, NCHC*H*N), 7.25 (t, 1H, $^3J_{HH}$ = 8 Hz, 2,6-($CH(CH_3)_2$)$_2$-C_6H_3), 7.11 (d, 2H,

https://doi.org/10.1021/acsomega.2c06729
ACS Omega 2023, 8, 6439−6454

$^3J_{HH}$ = 7 Hz, 2,6-(CH(CH$_3$)$_2$)$_2$-C$_6$H$_3$), 5.57 (s, 2H, CH$_2$), 4.16 (q, 2H, $^3J_{HH}$ = 7 Hz, CH$_2$CH$_3$), 3.03 (sept, 2H, $^3J_{HH}$ = 7 Hz, 2,6-(CH(CH$_3$)$_2$)$_2$-C$_6$H$_3$), 1.43 (t, 3H, $^3J_{HH}$ = 7 Hz, CH$_2$CH$_3$), 1.08 (br, 12H, 2,6-(CH(CH$_3$)$_2$)$_2$-C$_6$H$_3$). ^{13}C{^{1}H} NMR (CDCl$_3$, 125 MHz, 25 °C): δ ppm, 164.7 (CO), 146.1 (2,6-(CH(CH$_3$)$_2$)$_2$-C$_6$H$_3$), 136.7 (NCHN), 131.0 (2,6-(CH(CH$_3$)$_2$)$_2$-C$_6$H$_3$), 128.3 (2,6-(CH(CH$_3$)$_2$)$_2$-C$_6$H$_3$), 123.7 (NCHCHN), 123.2 (2,6-(CH(CH$_3$)$_2$)$_2$-C$_6$H$_3$), 121.2 (NCHCHN), 51.6 (CH$_2$), 45.1 (CH$_2$CH$_3$), 28.6 (2,6-(CH(CH$_3$)$_2$)$_2$-C$_6$H$_3$), 24.0 (2,6-(CH(CH$_3$)$_2$)$_2$-C$_6$H$_3$), 23.2 (2,6-(CH(CH$_3$)$_2$)$_2$-C$_6$H$_3$), 15.3 (CH$_2$CH$_3$). HRMS (ESI): Calcd. for [M − Cl]$^+$, [C$_{19}$H$_{28}$N$_3$O]$^+$ m/z 314.2227; found m/z 314.2229. Anal. Calcd. for C$_{19}$H$_{28}$N$_3$OCl: C, 65.22; H, 8.07; N, 12.01; Found: C, 64.85; H, 7.979; N, 11.40%.

Synthesis of [1-(Ethyl)-3-*N*-(2,6-di-*i*-propylphenylacetamido)-imidazol-2-ylidene]$_2$Ag$_2$ (3b). A solution of 1-(ethyl)-3-*N*-(2,6-di-*i*-propylphenyl)acetamido-imidazolium chloride (**3a**) (0.714 g, 2.04 mmol) in CH$_2$Cl$_2$ (ca. 40 mL) was stirred with Ag$_2$O (0.482 g, 2.07 mmol) in the dark at room temperature overnight. The solvent was evaporated, and the residue was purified by column chromatography on neutral Al$_2$O$_3$ using CHCl$_3$/CH$_3$OH (9.5:0.5 v/v) system to give the desired product (**3b**) as a white solid (0.324 g, 38%). ^{1}H NMR (CDCl$_3$, 500 MHz, 25 °C): δ ppm, 7.53 (s, 1H, NCHCHN), 7.06 (br s, 3H, 2,6-(CH(CH$_3$)$_2$)$_2$-C$_6$H$_3$), 6.93 (s, 1H, NCHCHN), 4.96 (s, 2H, CH$_2$), 3.88 (quat, 2H, $^3J_{HH}$ = 7 Hz, CH$_2$CH$_3$), 3.16 (sept, 2H, $^3J_{HH}$ = 7 Hz, 2,6-(CH(CH$_3$)$_2$)$_2$-C$_6$H$_3$), 1.26 (t, 3H, $^3J_{HH}$ = 7 Hz, CH$_2$CH$_3$), 1.15 (d, 6H, $^3J_{HH}$ = 7 Hz, 2,6-(CH(CH$_3$)$_2$)$_2$-C$_6$H$_3$), 1.06 (d, 6H, $^3J_{HH}$ = 7 Hz, 2,6-(CH(CH$_3$)$_2$)$_2$-C$_6$H$_3$). ^{13}C{^{1}H} NMR (CDCl$_3$, 125 MHz, 25 °C): δ ppm, 176.2 (d, ^1J ^{109}Ag−^{13}C$_{carbene}$ = 249 Hz, ^1J ^{107}Ag−^{13}C$_{carbene}$ = 219 Hz, Ag−NCN), 169.1 (CO), 143.6 (2,6-(CH(CH$_3$)$_2$)$_2$-C$_6$H$_3$), 142.5 (2,6-(CH(CH$_3$)$_2$)$_2$-C$_6$H$_3$), 124.6 (2,6-(CH(CH$_3$)$_2$)$_2$-C$_6$H$_3$), 123.1 (2,6-(CH(CH$_3$)$_2$)$_2$-C$_6$H$_3$), 122.9 (NCHCHN), 120.1 (NCHCHN), 61.8 (CH$_2$), 46.8 (CH$_2$CH$_3$), 28.1 (2,6-(CH(CH$_3$)$_2$)$_2$-C$_6$H$_3$), 23.9 (2,6-(CH(CH$_3$)$_2$)$_2$-C$_6$H$_3$), 23.8 (2,6-(CH(CH$_3$)$_2$)$_2$-C$_6$H$_3$), 16.9 (CH$_2$CH$_3$). IR data (cm^{-1}) KBr pellet: 3411 (w), 3124 (w), 2962 (m), 2867 (m), 1596 (s), 1574 (s), 1463 (w), 1438 (m), 1411 (m), 1225 (w), 752 (w). Anal. Calcd. for C$_{38}$H$_{52}$N$_6$O$_2$Ag$_2$: C, 54.30; H, 6.24; N, 10.00; Found: C, 54.80; H, 6.349; N, 9.96%.

Synthesis of [1-(Ethyl)-3-*N*-(2,6-di-*i*-propylphenylacetamido)-imidazol-2-ylidene]$_2$Au$_2$ (3c). [1-(Ethyl)-3-*N*-(2,6-di-*i*-propylphenylacetamido)-imidazol-2-ylidene]$_2$Ag$_2$ (**3b**) (0.151 g, 0.180 mmol) and (SMe$_2$)AuCl (0.107 g, 0.363 mmol) were mixed in CH$_2$Cl$_2$ and stirred for 6 h at room temperature. An off-white AgCl solid precipitated out during the course of reaction, after which it was filtered. The filtrate was dried under vacuum to give the crude product, which was purified by column chromatography on neutral Al$_2$O$_3$ using a mixed medium of CH$_2$Cl$_2$/CH$_3$OH (9.5:0.5, v/v) to give the product as a white-colored solid (**3c**) (0.076 g, 41%). ^{1}H NMR (CDCl$_3$, 400 MHz, 25 °C): δ ppm, 7.51 (d, 1H, $^3J_{HH}$ = 2 Hz, NCHCHN), 7.1 (s, 3H, 2,6-(CH(CH$_3$)$_2$)$_2$-C$_6$H$_3$), 6.84 (d, 1H, $^3J_{HH}$ = 2 Hz, NCHCHN), 5.29 (s, 2H, CH$_2$), 3.99 (q, 2H, $^3J_{HH}$ = 7 Hz, CH$_2$CH$_3$), 3.26 (sept, 2H, $^3J_{HH}$ = 7 Hz, 2,6-(CH(CH$_3$)$_2$)$_2$-C$_6$H$_3$), 1.32 (t, 3H, $^3J_{HH}$ = 7 Hz, CH$_2$CH$_3$), 1.21 (d, 6H, $^3J_{HH}$ = 7 Hz, 2,6-(CH(CH$_3$)$_2$)$_2$-C$_6$H$_3$), 1.02 (d, 6H, $^3J_{HH}$ = 7 Hz, 2,6-(CH(CH$_3$)$_2$)$_2$-C$_6$H$_3$). ^{13}C{^{1}H} NMR (CDCl$_3$, 100 MHz, 25 °C): δ ppm, 169.9 (NCN), 168.4 (CO), 143.4 (2,6-(CH(CH$_3$)$_2$)$_2$-C$_6$H$_3$), 141.9 (2,6-(CH(CH$_3$)$_2$)$_2$-C$_6$H$_3$), 125.5 (2,6-(CH(CH$_3$)$_2$)$_2$-C$_6$H$_3$), 122.9 (2,6-(CH(CH$_3$)$_2$)$_2$-C$_6$H$_3$), 122.4 (NCHCHN), 119.5 (NCHCHN), 58.8 (CH$_2$), 46.3 (CH$_2$CH$_3$), 27.7 (2,6-(CH(CH$_3$)$_2$)$_2$-C$_6$H$_3$), 24.1 (2,6-(CH(CH$_3$)$_2$)$_2$-C$_6$H$_3$), 23.8 (2,6-(CH(CH$_3$)$_2$)$_2$-C$_6$H$_3$), 16.5 (CH$_2$CH$_3$). IR data (cm^{-1}) KBr pellet: 3433 (br), 3127 (w), 2961 (m), 2866 (m), 1698 (s), 1598 (s), 1578 (s), 1465 (w), 1441 (m), 1416 (m), 1229 (w), 760 (w). HRMS (ESI): Calcd. for [M + H]$^+$, [C$_{38}$H$_{53}$N$_6$O$_2$Au$_2$]$^+$ m/z 1019.3556; found m/z 1019.3553. Anal. Calcd. for C$_{38}$H$_{52}$N$_6$O$_2$Au$_2$: C, 44.80; H, 5.14; N, 8.25; Found: C, 44.79; H, 5.143; N, 8.56%.

Synthesis of 1-(*i*-Propyl)-4-*N*-(2,6-di-*i*-propylphenylacetamido)-1,2,4-triazolium Chloride (4a). 1-*i*-Propyl 1,2,4-triazole (1.00 g, 9.04 mmol) and 2-chloro-N-(2,6-di-*i*-propylphenyl)acetamide (2.53 g, 9.97 mmol) were refluxed overnight in toluene (*ca.* 25 mL), after which the reaction mixture was cooled to room temperature. The solvent was evaporated, and the remaining solid was washed repeatedly with Et$_2$O to give a solid, which was purified by column chromatography on neutral silica using the CHCl$_3$/CH$_3$OH (9.5:0.5 v/v) system to give the product (**4a**) as a white solid (1.67 g, 51%). ^{1}H NMR (CDCl$_3$, 500 MHz, 25 °C): δ, 11.26 (s, 1H, NCHN), 10.63 (s, 1H, NH), 8.89 (s, 1H, NCHCHN), 7.26 (t, 1H, $^3J_{HH}$ = 8 Hz, 2,6-(CH(CH$_3$)$_2$)$_2$C$_6$H$_3$), 7.13 (d, 2H, $^3J_{HH}$ = 8 Hz, 2,6-(CH(CH$_3$)$_2$)$_2$C$_6$H$_3$), 5.88 (s, 2H, CH$_2$), 4.85 (sept, 1H, $^3J_{HH}$ = 7 Hz, NCH(CH$_3$)$_2$), 3.08 (sept, 2H, $^3J_{HH}$ = 7 Hz, 2,6-(CH(CH$_3$)$_2$)$_2$C$_6$H$_3$), 1.58 (d, 6H, $^3J_{HH}$ = 6 Hz, NCH(CH$_3$)$_2$), 1.13 (d, 12H, $^3J_{HH}$ = 6 Hz, 2,6-(CH(CH$_3$)$_2$)$_2$C$_6$H$_3$). ^{13}C{1H} NMR (CDCl$_3$, 125 MHz, 25 °C): δ ppm, 164.1 (CO), 145.9 (2,6-(CH(CH$_3$)$_2$)$_2$-C$_6$H$_3$), 144.5 (NC(5)HN), 141.9 (NC(3)HN), 130.9 (2,6-(CH(CH$_3$)$_2$)$_2$-C$_6$H$_3$), 128.3 (2,6-(CH(CH$_3$)$_2$)$_2$-C$_6$H$_3$), 123.3 (2,6-(CH(CH$_3$)$_2$)$_2$-C$_6$H$_3$), 56.2 (NCH(CH$_3$)$_2$), 50.1 (CH$_2$), 28.6 (2,6-(CH(CH$_3$)$_2$)$_2$-C$_6$H$_3$), 24.1 (2,6-(CH(CH$_3$)$_2$)$_2$-C$_6$H$_3$), 23.2 (2,6-(CH(CH$_3$)$_2$)$_2$-C$_6$H$_3$), 21.7 (NCH(CH$_3$)$_2$). IR data (cm^{-1}) KBr pellet: 3441 (w), 3195 (m), 2964 (s), 2931 (m), 1697 (s), 1530 (m), 1468 (m), 1360 (w), 1238 (m), 1057 (w), 984 (m), 715 (w). HRMS (ESI): Calcd. for [M − Cl]$^+$, [C$_{19}$H$_{29}$N$_4$O]$^+$ m/z 329.2336; found m/z 329.2334. Anal. Calcd. for C$_{19}$H$_{29}$N$_4$OCl: C, 62.54; H, 8.01; N, 15.35; Found: C, 62.65; H, 7.905; N, 15.44%.

Synthesis of [1-(*i*-Propyl)-4-*N*-(2,6-di-*i*-propylphenylacetamido)-1,2,4-triazol-2-ylidene]$_2$Ag$_2$ (4b). A solution of 1-(*i*-propyl)-4-N-(2,6-di-*i*-propylphenyl)acetamido-1,2,4-triazolium chloride (**4a**) (0.502 g, 1.37 mmol) in CH$_2$Cl$_2$ (ca. 40 mL) was stirred with Ag$_2$O (0.329 g, 1.42 mmol) in the dark at room temperature overnight. The solvent was evaporated, and the residue was purified by column chromatography on neutral Al$_2$O$_3$ using the CHCl$_3$:CH$_3$OH (9.5:0.5) system to give the product (**4b**) as a gray solid (0.207 g, 34%). ^{1}H NMR (CDCl$_3$, 500 MHz, 25 °C): δ ppm, 8.46 (s, 1H, NCHN), 7.24 (t, 1H, $^3J_{HH}$ = 8 Hz, 2,6-(CH(CH$_3$)$_2$)$_2$-C$_6$H$_3$), 7.10 (d, 2H, $^3J_{HH}$ = 7 Hz, 2,6-(CH(CH$_3$)$_2$)$_2$-C$_6$H$_3$), 5.52 (s, 2H, CH$_2$), 4.97 (sept, 1H, $^3J_{HH}$ = 7 Hz, NCH(CH$_3$)$_2$), 3.00 (sept, 2H, $^3J_{HH}$ = 7 Hz, 2,6-(CH(CH$_3$)$_2$)$_2$-C$_6$H$_3$), 1.58 (d, 6H, $^3J_{HH}$ = 7 Hz, NCH(CH$_3$)$_2$), 1.06 (d, 12H, $^3J_{HH}$ = 7 Hz, 2,6-(CH(CH$_3$)$_2$)$_2$-C$_6$H$_3$). ^{13}C{^{1}H} NMR (CDCl$_3$, 125 MHz, 25 °C): δ ppm, 180.9 (s, Ag−NCN), 166.0 (CO), 145.8 (2,6-(CH(CH$_3$)$_2$)$_2$-C$_6$H$_3$), 143.3 (NCHN), 130.8 (2,6-(CH(CH$_3$)$_2$)$_2$-C$_6$H$_3$), 128.3 (2,6-(CH(CH$_3$)$_2$)$_2$-C$_6$H$_3$), 123.3 (2,6-(CH(CH$_3$)$_2$)$_2$-C$_6$H$_3$), 56.3 (NCH(CH$_3$)$_2$), 51.3 (CH$_2$), 28.6 (2,6-(CH(CH$_3$)$_2$)$_2$-C$_6$H$_3$), 23.6 (2,6-(CH(CH$_3$)$_2$)$_2$-C$_6$H$_3$), 22.8 (NCH(CH$_3$)$_2$). IR data

https://doi.org/10.1021/acsomega.2c06729
ACS Omega 2023, 8, 6439−6454

(cm^{-1}) KBr pellet: 3512 (m), 3190 (m), 2964 (s), 2869 (m), 1677 (m), 1590 (s), 1531 (s), 1444 (m), 1383 (m), 976 (w), 797 (w), 722 (w). Anal. Calcd. for $C_{38}H_{54}N_8O_2Ag_2$: C, 52.42; H, 6.25; N, 12.87; Found: C, 52.37; H, 6.366; N, 12.57%.

Synthesis of [1-(*i*-Propyl)-4-*N*-(2,6-di-*i*-propylphenylacetamido)-1,2,4-triazol-2-ylidene]$_2$Au$_2$ (4c). [1-(*i*-Propyl)-4-*N*-(2,6-di-*i*-propylphenylacetamido)-1,2,4-triazol-2-ylidene]$_2$Ag$_2$ (**4b**) (0.120 g, 0.138 mmol) and (SMe_2)AuCl (0.082 g, 0.280 mmol) were mixed in CH_2Cl_2 and stirred for 6 h at room temperature. An off-white AgCl solid precipitated out during the course of reaction, after which it was filtered. The filtrate was dried under vacuum to give the crude product, which was purified by column chromatography on neutral Al_2O_3 using a mixed medium of CH_2Cl_2/CH_3OH (9.5:0.5, v/v) to give the product as a white-colored solid (**4c**) (0.038 g, 26%). ^{1}H NMR ($CDCl_3$, 500 MHz, 25 °C): δ ppm, 8.33 (s, 1H, NC*H*N), 7.30 (t, 1H, $^3J_{HH}$ = 8 Hz, 2,6-(CH(CH_3)$_2$)$_2$-C_6H_3), 7.15 (d, 2H, $^3J_{HH}$ = 7 Hz, 2,6-(CH(CH_3)$_2$)$_2$-C_6H_3), 5.12−5.06 (m, 3H, CH_2 and NCH(CH_3)$_2$), 3.07 (sept, 2H, $^3J_{HH}$ = 7 Hz, 2,6-(CH(CH_3)$_2$)$_2$-C_6H_3), 1.49 (d, 6H, $^3J_{HH}$ = 7 Hz, NCH(CH_3)$_2$), 1.16 (d, 12H, $^3J_{HH}$ = 7 Hz, 2,6-(CH(CH_3)$_2$)$_2$-C_6H_3). ^{13}C{^{1}H} NMR ($CDCl_3$, 125 MHz, 25 °C): δ ppm, 171.8 (N*C*N), 164.7 (*C*O), 146.2 (2,6-(CH(CH_3)$_2$)$_2$-*C*$_6H_3$), 143.3 (N*C*HN), 129.8 (2,6-(CH(CH_3)$_2$)$_2$-*C*$_6H_3$), 128.8 (2,6-(CH(CH_3)$_2$)$_2$-*C*$_6H_3$), 123.5 (2,6-(CH(CH_3)$_2$)$_2$-*C*$_6H_3$), 55.9 (N*C*H(CH_3)$_2$), 51.0 (CH_2), 28.8 (2,6-(*C*H(CH_3)$_2$)$_2$-C_6H_3), 23.7 (2,6-(CH(*C*H$_3$)$_2$)$_2$-C_6H_3), 22.2 (NCH(*C*H$_3$)$_2$). IR data (cm^{-1}) KBr pellet: 3482 (br), 3122 (w), 2965 (m), 1672 (s), 1521 (s), 1451 (m), 796 (m), 718 (w). HRMS (ESI): Calcd. for $[M + H]^+$, $[C_{38}H_{55}N_8O_2Au_2]^+$ m/z 1049.3774; found m/z 1049.3770. Anal. Calcd. for $C_{38}H_{54}N_8O_2Au_2$: C, 43.52; H, 5.19; N, 10.68; Found: C, 42.95; H, 5.457; N, 10.03%.

General Procedure for Photophysical Study. Using a Shimadzu UV−NIR instrument, absorption spectra of compounds **1**(**a**−**c**), **2**(**a**−**c**), **3**(**a**−**c**), and **4**(**a**−**c**) were recorded in $CHCl_3$ solution (1×10^{-3} M) at 25 °C. Using a Varian Eclipse spectrophotometer, emission spectra of compounds **1**(**a**−**c**), **2**(**a**−**c**), **3**(**a**−**c**), and **4**(**a**−**c**) were recorded in $CHCl_3$ solution (1×10^{-3} M) at 25 °C upon excitation at 242 nm in quartz cuvettes. Solid-state emission was recorded on a Horiba Fluoromax + (RM 360) instrument at 25 °C upon excitation at 242 nm in quartz glass slab for the compounds **1**(**a**−**c**), **2**(**a**−**c**), **3**(**a**−**c**), and **4**(**a**−**c**) by mixing with NaCl in the ratio of 1:100 and grinding the mixture to a powder form.

Computational Methods. DFT calculations were done using the Gaussian 09 suite of the programs.[55] All calculations were performed using the UB3LYP-D2[56] functional in conjunction with an all-electron def2-TZVP[57] basis set for all atoms. To take into consideration the relativistic effects, Douglas−Kroll−Hess (DKH) Hamiltonian[58] has been employed. To avoid the lattice effects on the geometry, X-ray structures were utilized as such. And single-point calculations, including relativistic effects, were performed, and the generated wavefunction was further used for the natural bond orbital (NBO).[59] However, we assumed that intermolecular interactions present in the crystal have no significant impact on the metallophilic interactions. To comprehend the metallophilic interactions, the atoms in molecules (AIM) analysis,[60] electron localization function (ELF),[44] and noncovalent interaction (NCI)[41] analyses were carried out on all complexes using Multiwfn software.[61] Isosurfaces of the reduced density gradient (RDG)[42] were rendered by the VMD 1.9.1 program[62] using the output files of Multiwfn.[61]

Using the polarized continuum model and TD-DFT at the PBE1PBE[63] hybrid functional level, which includes 25% exchange and 75% correlation in chloroform ($CHCl_3$) media, the absorption properties were estimated. It has been demonstrated that this level of the theoretical approach is trustworthy for 5d transition-metal complex systems.[64] Finally, a natural transition orbital (NTO) analysis was carried out to better understand the nature of excited states involved in absorption processes.[65]

■ ASSOCIATED CONTENT

Supporting Information

The Supporting Information is available free of charge at https://pubs.acs.org/doi/10.1021/acsomega.2c06729.

^{1}H NMR, ^{13}C{^{1}H} NMR, IR, HRMS, and CHN data of the amido-functionalized NHC ligands **1a**−**4a**; ^{1}H NMR, ^{13}C{1H} NMR, IR, CHN data, and the computational data of the silver **1b**−**4b**; ^{1}H NMR, ^{13}C{^{1}H} NMR, IR, HRMS, CHN data, and the computational data of gold **1c**−**4c** complexes; and emission spectra for the silver **1b**−**4b** and gold **1c**−**4c** complexes (PDF)

■ AUTHOR INFORMATION

Corresponding Authors

Gopalan Rajaraman − *Department of Chemistry, Indian Institute of Technology Bombay, Mumbai 400076, India;* orcid.org/0000-0001-6133-3026; Email: rajaraman@chem.iitb.ac.in

Prasenjit Ghosh − *Department of Chemistry, Indian Institute of Technology Bombay, Mumbai 400076, India;* orcid.org/0000-0002-9479-8177; Email: pghosh@chem.iitb.ac.in; Fax: +91 22 2572 3480

Authors

A. P. Prakasham − *Department of Chemistry, Indian Institute of Technology Bombay, Mumbai 400076, India;* Present Address: Laboratory of Macromolecular and Organic Chemistry, Institute for Complex Molecular Systems, Department of Chemical Engineering and Chemistry, Eindhoven University of Technology, 5600 MB Eindhoven, The Netherlands; orcid.org/0000-0001-7651-679X

Sagar K. Patil − *Department of Chemistry, Indian Institute of Technology Bombay, Mumbai 400076, India*

Chandrasekhar Nettem − *Department of Chemistry, Indian Institute of Technology Bombay, Mumbai 400076, India*

Shreyata Dey − *Department of Chemistry, Indian Institute of Technology Bombay, Mumbai 400076, India;* orcid.org/0000-0003-1600-7402

Complete contact information is available at: https://pubs.acs.org/10.1021/acsomega.2c06729

Author Contributions

†A.P.P., S.K.P., and C.N. contributed equally to this work.

Notes

The authors declare no competing financial interest.

https://doi.org/10.1021/acsomega.2c06729
ACS Omega 2023, 8, 6439−6454

■ ACKNOWLEDGMENTS

The authors acknowledge the Department of Science and Technology (DST), India (Grant Nos. SR/S1/IC-50/2011, EMR/2014/000254, CRG/2019/000029) and Council for Scientific and Industrial Research (CSIR), New Delhi, (01(2880)/17/EMR-II) India for financial support. The Single-Crystal X-ray Diffraction Facility, Department of Chemistry, IIT Bombay is gratefully acknowledged for the crystallographic characterization data. A.P.P. thanks CSIR, New Delhi and C.N. S.K.P. and S.R.D. thank IIT Bombay for a research fellowship.

■ REFERENCES

(1) Sculfort, S.; Braunstein, P. Intramolecular d10−d10 interactions in heterometallic clusters of the transition metals. *Chem. Soc. Rev.* **2011**, *40*, 2741−2760. Pyykkö, P. Theoretical Chemistry of Gold. *Angew. Chem., Int. Ed.* **2004**, *43*, 4412−4456.

(2) Pyykkö, P. Strong Closed-Shell Interactions in Inorganic Chemistry. *Chem. Rev.* **1997**, *97*, 597−636.

(3) Vijayaraghavan, R. K.; Chandran, D.; Vijayaraghavan, R. K.; McCoy, A. P.; Daniels, S.; McNally, P. J. Highly enhanced UV responsive conductivity and blue emission in transparent CuBr films: implication for emitter and dosimeter applications. *J. Mater. Chem. C* **2017**, *5*, 10270−10279. Kishimura, A.; Yamashita, T.; Yamaguchi, K.; Aida, T. Rewritable phosphorescent paper by the control of competing kinetic and thermodynamic self-assembling events. *Nat. Mater.* **2005**, *4*, 546−549.

(4) Henkelis, J. J.; Barnett, S. A.; Harding, L. P.; Hardie, M. J. Coordination Polymers Utilizing N-Oxide Functionalized Host Ligands. *Inorg. Chem.* **2012**, *51*, 10657−10674. Serpe, A.; Artizzu, F.; Marchiò, L.; Mercuri, M. L.; Pilia, L.; Deplano, P. Argentophilic Interactions in Mono-, Di-, and Polymeric Ag(I) Complexes with N,N′-Dimethyl-piperazine-2,3-dithione and Iodide. *Cryst. Growth Des.* **2011**, *11*, 1278−1286. Bayler, A.; Schier, A.; Bowmaker, G. A.; Schmidbaur, H. Gold Is Smaller than Silver. Crystal Structures of [Bis(trimesitylphosphine)gold(I)] and [Bis(trimesitylphosphine)-silver(I)] Tetrafluoroborate. *J. Am. Chem. Soc.* **1996**, *118*, 7006−7007.

(5) Gil-Rubio, J.; Vicente, J. The Coordination and Supramolecular Chemistry of Gold Metalloligands. *Chem. − Eur. J.* **2018**, *24*, 32−46. Yam, V. W.-W.; Wong, K. M.-C. Luminescent metal complexes of d6, d8 and d10 transition metal centres. *Chem. Commun.* **2011**, *47*, 11579−11592.

(6) Jassal, A. K. Advances in ligand-unsupported argentophilic interactions in crystal engineering: an emerging platform for supramolecular architectures. *Inorg. Chem. Front.* **2020**, *7*, 3735−3764.

(7) Zheng, J.; Lu, Z.; Wu, K.; Ning, G.-H.; Li, D. Coinage-Metal-Based Cyclic Trinuclear Complexes with Metal−Metal Interactions: Theories to Experiments and Structures to Functions. *Chem. Rev.* **2020**, *120*, 9675−9742.

(8) Yam, V. W.-W.; Au, V. K.-M.; Leung, S. Y.-L. Light-Emitting Self-Assembled Materials Based on d8 and d10 Transition Metal Complexes. *Chem. Rev.* **2015**, *115*, 7589−7728. Yang, C.; Elbjeirami, O.; Gamage, C. S. P.; Dias, H. V. R.; Omary, M. A. Luminescence enhancement and tuning via multiple cooperative supramolecular interactions in an ion-paired multinuclear complex. *Chem. Commun.* **2011**, *47*, 7434−7436.

(9) Rana, A.; Kumar Jana, S.; Pal, T.; Puschmann, H.; Zangrando, E.; Dalai, S. Electrical conductivity and luminescence properties of two silver(I) coordination polymers with heterocyclic nitrogen ligands. *J. Solid State Chem.* **2014**, *216*, 49−55. Dennehy, M.; Amo-Ochoa, P.; Freire, E.; Suárez, S.; Halac, E.; Baggio, R. Structure and electrical properties of a one-dimensional polymeric silver thio-saccharinate complex with argentophilic interactions. *Acta Crystallogr., Sect. C: Struct. Chem.* **2018**, *74*, 186−193.

(10) Schmidbaur, H.; Schier, A. Argentophilic Interactions. *Angew. Chem., Int. Ed.* **2015**, *54*, 746−784.

(11) Schmidbaur, H.; Schier, A. Aurophilic interactions as a subject of current research: an up-date. *Chem. Soc. Rev.* **2012**, *41*, 370−412.

(12) Schmidbaur, H.; Raubenheimer, H. G. Excimer and Exciplex Formation in Gold(I) Complexes Preconditioned by Aurophilic Interactions. *Angew. Chem., Int. Ed.* **2020**, *59*, 14748−14771.

(13) Harisomayajula, N. V. S.; Makovetskyi, S.; Tsai, Y.-C. Cuprophilic Interactions in and between Molecular Entities. *Chem. − Eur. J.* **2019**, *25*, 8936−8954.

(14) Jung, O.-S.; Kim, Y. J.; Lee, Y.-A.; Kang, S. W.; Choi, S. N. Tunable Transannular Silver−Silver Interaction in Molecular Rectangles. *Cryst. Growth Des.* **2004**, *4*, 23−24.

(15) Alvarez, S. A cartography of the van der Waals territories. *Dalton Trans.* **2013**, *42*, 8617−8636. Hu, S.-Z.; Zhou, Z.-H.; Robertson, B. E. Consistent approaches to van der Waals radii for the metallic elements. *Z. Kristallogr.* **2009**, *224*, 375−383. Mantina, M.; Chamberlin, A. C.; Valero, R.; Cramer, C. J.; Truhlar, D. G. Consistent van der Waals Radii for the Whole Main Group. *J. Phys. Chem. A* **2009**, *113*, 5806−5812.

(16) Bondi, A. van der Waals volumes and radii. *J. Phys. Chem. A* **1964**, *68*, 441−451.

(17) Batsanov, S. S. Van der Waals Radii of Elements. *Inorg. Mater.* **2001**, *37*, 871−885.

(18) Korneeva, E. V.; Smolentsev, A. I.; Antzutkin, O. N.; Ivanov, A. V. A novel silver(I) di-iso-butyldithiocarbamate: Unusually complicated 1-D polymeric structure, multiple ligand-supported Ag−Ag interactions and its capability to bind gold(III). Preparation, structural organisation and (13C, 15N) CP-MAS NMR of [Ag6(S2CNiBu2)6]n and [Au(S2CNiBu2)2][AgCl2]. *Inorg. Chim. Acta* **2021**, *525*, No. 120383. Vikulova, E. S.; Sukhikh, T. S.; Gulyaev, S. A.; Ilyin, I. Y.; Morozova, N. B. Structural Diversity of Silver Fluorinated *β*-Diketonates: Effect of the Terminal Substituent and Solvent. *Molecules* **2022**, *27*, No. 677. Xia, C.-K.; Min, Y.-Y.; Yang, K.; Sun, W.; Jiang, D.-L.; Chen, M. Syntheses, Crystal Structures, and Properties of Three Novel Silver−Organic Frameworks Assembled from 1,2,3,5-Benzene-tetracarboxylic Acid Based on Argentophilic Interactions. *Cryst. Growth Des.* **2018**, *18*, 1978−1986. Che, C.-M.; Tse, M.-C.; Chan, M. C. W.; Cheung, K.-K.; Phillips, D. L.; Leung, K.-H. Spectroscopic Evidence for Argentophilicity in Structurally Characterized Luminescent Binuclear Silver(I) Complexes. *J. Am. Chem. Soc.* **2000**, *122*, 2464−2468. Kobialka, S.; Müller-Tautges, C.; Schmidt, M. T. S.; Schnakenburg, G.; Hollóczki, O.; Kirchner, B.; Engeser, M. Stretch Out or Fold Back? Conformations of Dinuclear Gold(I) N-Heterocyclic Carbene Macrocycles. *Inorg. Chem.* **2015**, *54*, 6100−6111. Monticelli, M.; Baron, M.; Tubaro, C.; Bellemin-Laponnaz, S.; Graiff, C.; Bottaro, G.; Armelao, L.; Orian, L. Structural and Luminescent Properties of Homoleptic Silver(I), Gold(I), and Palladium(II) Complexes with nNHC-tzNHC Heteroditopic Carbene Ligands. *ACS Omega* **2019**, *4*, 4192−4205. Espada, M. F.; Campos, J.; López-Serrano, J.; Poveda, M. L.; Carmona, E. Methyl-, Ethenyl-, and Ethynyl-Bridged Cationic Digold Complexes Stabilized by Coordination to a Bulky Terphenylphosphine Ligand. *Angew. Chem., Int. Ed.* **2015**, *54*, 15379−15384. (acccessed 2022/06/30) Nakamura, T.; Ogushi, S.; Arikawa, Y.; Umakoshi, K. Preparations of a series of coinage metal complexes with pyridine-based bis(N-heterocyclic carbene) ligands including transmetalation to palladium complexes. *J. Organomet. Chem.* **2016**, *803*, 67−72.

(19) Ray, L.; Shaikh, M. M.; Ghosh, P. Shorter argentophilic interaction than aurophilic interaction in a pair of dimeric {(NHC)MCl}(2) (M= Ag, Au) complexes supported over a N/O-functionalized N-heterocyclic carbene (NHC) ligand. *Inorg. Chem.* **2008**, *47*, 230−240.

(20) Pilar Carranza, M.; Manzano, B. R.; Jalón, F. A.; Rodríguez, A. M.; Santos, L.; Moreno, M. Experimental and theoretical evidence of unsupported Ag−Ag interactions in complexes with triazine-based ligands. Subtle effects of the symmetry of the triazine substituents. *New J. Chem.* **2013**, *37*, 3183−3194. Baron, M.; Dalla Tiezza, M.; Carlotto, A.; Tubaro, C.; Graiff, C.; Orian, L. Di(N-heterocyclic carbene) gold(III) imidate complexes obtained by oxidative addition of N-halosuccinimides. *J. Organomet. Chem.* **2018**, *866*, 144−152.

https://doi.org/10.1021/acsomega.2c06729
ACS Omega 2023, 8, 6439−6454

(21) Schmidbaur, H.; Graf, W.; Müller, G. Weak Intramolecular Bonding Relationships: The Conformation-Determining Attractive Interaction between Gold(I) Centers. *Angew. Chem., Int. Ed.* **1988**, *27*, 417−419.
(22) Schmidbaur, H. The fascinating implications of new results in gold chemistry. *Gold Bull.* **1990**, *23*, 11−21. Jiang, Y.; Alvarez, S.; Hoffmann, R. Binuclear and polymeric gold(I) complexes. *Inorg. Chem.* **1985**, *24*, 749−757. Jansen, M. Homoatomic d10−d10 Interactions: Their Effects on Structure and Chemical and Physical Properties. *Angew. Chem., Int. Ed.* **1987**, *26*, 1098−1110.
(23) Schmidbaur, H. The aurophilicity phenomenon: A decade of experimental findings, theoretical concepts and emerging applications. *Gold Bull.* **2000**, *33*, 3−10.
(24) Andris, E.; Andrikopoulos, P. C.; Schulz, J.; Turek, J.; Růžička, A.; Roithová, J.; Rulíšek, L. Aurophilic Interactions in [(L)AuCl]··· [(L′)AuCl] Dimers: Calibration by Experiment and Theory. *J. Am. Chem. Soc.* **2018**, *140*, 2316−2325.
(25) Zheng, Q.; Borsley, S.; Nichol, G. S.; Duarte, F.; Cockroft, S. L. The Energetic Significance of Metallophilic Interactions. *Angew. Chem., Int. Ed.* **2019**, *58*, 12617−12623.
(26) Andrejić, M.; Mata, R. A. Study of ligand effects in aurophilic interactions using local correlation methods. *Phys. Chem. Chem. Phys.* **2013**, *15*, 18115−18122. Mirzadeh, N.; Privér, S. H.; Blake, A. J.; Schmidbaur, H.; Bhargava, S. K. Innovative Molecular Design Strategies in Materials Science Following the Aurophilicity Concept. *Chem. Rev.* **2020**, *120*, 7551−7591.
(27) Schmidbaur, H.; Schier, A. A briefing on aurophilicity. *Chem. Soc. Rev.* **2008**, *37*, 1931−1951.
(28) Liu, R.-F.; Franzese, C. A.; Malek, R.; Żuchowski, P. S.; Ángyán, J. G.; Szczęśniak, M. M.; Chałasiński, G. Aurophilic Interactions from Wave Function, Symmetry-Adapted Perturbation Theory, and Rangehybrid Approaches. *J. Chem. Theory Comput.* **2011**, *7*, 2399−2407. Riedel, S.; Pyykkö, P.; Mata, R. A.; Werner, H.-J. Comparative calculations for the A-frame molecules [S(MPH3)2] (M=Cu, Ag, Au) at levels up to CCSD(T). *Chem. Phys. Lett.* **2005**, *405*, 148−152.
(29) Pyykkö, P.; Zhao, Y. Ab initio Calculations on the (ClAuPH3)2 Dimer with Relativistic Pseudopotential: Is the "Aurophilic Attraction" a Correlation Effect? *Angew. Chem., Int. Ed.* **1991**, *30*, 604−605.
(30) Magnko, L.; Schweizer, M.; Rauhut, G.; Schütz, M.; Stoll, H.; Werner, H.-J. A comparison of metallophilic attraction in (X−M−PH3)2 (M = Cu, Ag, Au; X = H, Cl). *Phys. Chem. Chem. Phys.* **2002**, *4*, 1006−1013.
(31) O'Grady, E.; Kaltsoyannis, N. Does metallophilicity increase or decrease down group 11? Computational investigations of [Cl−M−PH3]2 (M = Cu, Ag, Au, [111]). *Phys. Chem. Chem. Phys.* **2004**, *6*, 680−687.
(32) Kumar, D.; Prakasham, A. P.; Das, S.; Datta, A.; Ghosh, P. Cyanosilylation of Aromatic Aldehydes by Cationic Ruthenium(II) Complexes of Benzimidazole-Derived O-Functionalized N-Heterocyclic Carbenes at Ambient Temperature under Solvent-Free Conditions. *ACS Omega* **2018**, *3*, 1922−1938.
(33) Samantaray, M. K.; Pang, K.; Shaikh, M. M.; Ghosh, P. From large 12-membered macrometallacycles to ionic (NHC)(2)M+Cl- type complexes of gold and silver by modulation of the N-substituent of amido-functionalized N-heterocyclic carbene (NHC) Ligands. *Inorg. Chem.* **2008**, *47*, 4153−4165.
(34) Shmelev, N. Y.; Okubazghi, T. H.; Abramov, P. A.; Komarov, V. Y.; Rakhmanova, M. I.; Novikov, A. S.; Gushchin, A. L. Intramolecular aurophilic interactions in dinuclear gold(i) complexes with twisted bridging 2,2′-bipyridine ligands. *Dalton Trans.* **2021**, *50*, 12448−12456. Krätschmer, F.; Gui, X.; Gamer, M. T.; Klopper, W.; Roesky, P. W. Systematic investigation of the influence of electronic substituents on dinuclear gold(i) amidinates: synthesis, characterisation and photoluminescence studies. *Dalton Trans.* **2022**, *51*, 5471−5479.
(35) Tripathi, U. M.; Bauer, A.; Schmidbaur, H. Covalent radii of four-co-ordinate copper(I), silver(I) and gold(I): crystal structures of [Ag(AsPh3)4]BF4 and [Au(AsPh3)4]BF4. *J. Chem. Soc., Dalton Trans.* **1997**, 2865−2868.
(36) Leang, S. S.; Zahariev, F.; Gordon, M. S. Benchmarking the performance of time-dependent density functional methods. *J. Chem. Phys.* **2012**, *136*, No. 104101. Jacquemin, D.; Perpète, E. A.; Scuseria, G. E.; Ciofini, I.; Adamo, C. TD-DFT Performance for the Visible Absorption Spectra of Organic Dyes: Conventional versus Long-Range Hybrids. *J. Chem. Theory Comput.* **2008**, *4*, 123−135.
(37) Brands, M. B.; Nitsch, J.; Guerra, C. F. Relevance of Orbital Interactions and Pauli Repulsion in the Metal−Metal Bond of Coinage Metals. *Inorg. Chem.* **2018**, *57*, 2603−2608.
(38) Gatfaoui, S.; Sagaama, A.; Issaoui, N.; Roisnel, T.; Marouani, H. Synthesis, experimental, theoretical study and molecular docking of 1-ethylpiperazine-1,4-diium bis(nitrate). *Solid State Sci.* **2020**, *106*, No. 106326.
(39) Puyo, M.; Lebon, E.; Vendier, L.; Kahn, M. L.; Fau, P.; Fajerwerg, K.; Lepetit, C. Topological Analysis of Ag−Ag and Ag−N Interactions in Silver Amidinate Precursor Complexes of Silver Nanoparticles. *Inorg. Chem.* **2020**, *59*, 4328−4339.
(40) Dey, S.; Velmurugan, G.; Rajaraman, G. How important is the coordinating atom in controlling magnetic anisotropy in uranium(iii) single-ion magnets? A theoretical perspective. *Dalton Trans.* **2019**, *48*, 8976−8988.
(41) Johnson, E. R.; Keinan, S.; Mori-Sánchez, P.; Contreras-García, J.; Cohen, A. J.; Yang, W. Revealing Noncovalent Interactions. *J. Am. Chem. Soc.* **2010**, *132*, 6498−6506.
(42) Contreras-García, J.; Johnson, E. R.; Keinan, S.; Chaudret, R.; Piquemal, J.-P.; Beratan, D. N.; Yang, W. NCIPLOT: A Program for Plotting Noncovalent Interaction Regions. *J. Chem. Theory Comput.* **2011**, *7*, 625−632.
(43) Wan, Q.; Yang, J.; To, W.-P.; Che, C.-M. Strong metal−metal Pauli repulsion leads to repulsive metallophilicity in closed-shell d8 and d10 organometallic complexes. *Proc. Natl. Acad. Sci. U.S.A.* **2021**, *118*, No. e2019265118.
(44) Becke, A. D.; Edgecombe, K. E. A simple measure of electron localization in atomic and molecular systems. *J. Chem. Phys.* **1990**, *92*, 5397−5403. (acccessed 2022/06/29).
(45) Savin, A. The electron localization function (ELF) and its relatives: interpretations and difficulties. *THEOCHEM* **2005**, *727*, 127−131.
(46) Koumpouras, K.; Larsson, J. A. Distinguishing between chemical bonding and physical binding using electron localization function (ELF). *J. Phys.: Condens. Matter* **2020**, *32*, No. 315502.
(47) Schmider, H. L.; Becke, A. D. Chemical content of the kinetic energy density. *THEOCHEM* **2000**, *527*, 51−61.
(48) Jacobsen, H. Localized-orbital locator (LOL) profiles of chemical bonding. *Can. J. Chem.* **2008**, *86*, 695−702.
(49) Kender, W. T.; Turro, C. Unusually Slow Internal Conversion in N-Heterocyclic Carbene/Carbanion Cyclometallated Ru(II) Complexes: A Hammett Relationship. *J. Phys. Chem. A* **2019**, *123*, 2650−2660.
(50) Mas-Marzá, E.; Peris, E.; Castro-Rodríguez, I.; Meyer, K. Synthesis and Catalytic Properties of Two Trinuclear Complexes of Rhodium and Iridium with the N-Heterocyclic Tris-carbene Ligand TIMENiPr. *Organometallics* **2005**, *24*, 3158−3162.
(51) Dash, C.; Shaikh, M. M.; Ghosh, P. Silver complexes of 1,2,4-triazole derived N-heterocyclic carbenes: Synthesis, structure and reactivity studies. *J. Chem. Sci.* **2011**, *123*, 97−106.
(52) Paczal, A.; Benyei, A. C.; Kotschy, A. Modular Synthesis of Heterocyclic Carbene Precursors. *J. Org. Chem.* **2006**, *71*, 5969−5979.
(53) Brandys, M.-C.; Jennings, M. C.; Puddephatt, R. J. Luminescent gold(I) macrocycles with diphosphine and 4,4′-bipyridyl ligands. *J. Chem. Soc., Dalton Trans.* **2000**, 4601−4606.
(54) Sheldrick, G. M. A short history of SHELX. *Acta Crystallogr., Sect. A: Found. Crystallogr.* **2008**, *64*, 112−122.
(55) Frisch, M. J.; Trucks, G. W.; Schlegel, H. B.; Scuseria, G. E.; Robb, M. A.; Cheeseman, J. R.; Scalmani, G.; Barone, V; Mennucci, B.; Petersson, G. A. et al. *Gaussian 09*, revision A.1; Gaussian, Inc.: Wallingford, CT, 2009.

https://doi.org/10.1021/acsomega.2c06729
ACS Omega 2023, 8, 6439−6454

(56) Becke, A. D. Density-functional exchange-energy approximation with correct asymptotic behavior. *Phys. Rev. A* **1988**, *38*, 3098−3100.
(57) Weigend, F.; Ahlrichs, R. Balanced basis sets of split valence, triple zeta valence and quadruple zeta valence quality for H to Rn: Design and assessment of accuracy. *Phys. Chem. Chem. Phys.* **2005**, *7*, 3297−3305.
(58) Reiher, M. Douglas−Kroll−Hess Theory: a relativistic electrons-only theory for chemistry. *Theor. Chem. Acc.* **2006**, *116*, 241−252.
(59) Reed, A. E.; Curtiss, L. A.; Weinhold, F. Intermolecular interactions from a natural bond orbital, donor-acceptor viewpoint. *Chem. Rev.* **1988**, *88*, 899−926.
(60) Bader, R. F. W. Atoms in molecules. *Acc. Chem. Res.* **1985**, *18*, 9−15.
(61) Lu, T.; Chen, F. Multiwfn: A multifunctional wavefunction analyzer. *J. Comput. Chem.* **2012**, *33*, 580−592.
(62) Humphrey, W.; Dalke, A.; Schulten, K. VMD: Visual molecular dynamics. *J. Mol. Graphics* **1996**, *14*, 33−38.
(63) Adamo, C.; Barone, V. Toward reliable density functional methods without adjustable parameters: The PBE0 model. *J. Chem. Phys.* **1999**, *110*, 6158−6170.
(64) Velmurugan, G.; Ramamoorthi, B. K.; Venuvanalingam, P. Are Re(i) phenanthroline complexes suitable candidates for OLEDs? Answers from DFT and TD-DFT investigations. *Phys. Chem. Chem. Phys.* **2014**, *16*, 21157−21171. Velmurugan, G.; Venuvanalingam, P. Luminescent Re(i) terpyridine complexes for OLEDs: what does the DFT/TD-DFT probe reveal? *Dalton Trans.* **2015**, *44*, 8529−8542.
(65) Martin, R. L. Natural transition orbitals. *J. Chem. Phys.* **2003**, *118*, 4775−4777.

Recommended by ACS

Accessing Heteroannular Benzoxazole and Benzimidazole Scaffolds via Carbodiimides Using Azide–Isocyanide Cross-Coupling as Catalyzed by Mesoionic Singlet Palladium C...

Shreyata Dey and Prasenjit Ghosh
MARCH 14, 2023
ACS OMEGA
READ

Influence of the Steric/Electronic Properties of *N*-Aryl Substituents in Cycloplatinated Guanidinate(1−) Complexes on the Formation of Discrete Pt → Ag Complexes and On...

Nitish Kumar Sinha, Natesan Thirupathi, *et al.*
MAY 02, 2023
INORGANIC CHEMISTRY
READ

Copper(I), Silver(I), and Gold(I) Ethylene Complexes of Fluorinated and Boron-Methylated Bis- and Tris(pyridyl)borate Chelators

Brandon T. Watson, H. V. Rasika Dias, *et al.*
JANUARY 19, 2023
INORGANIC CHEMISTRY
READ

Noncovalent Chelation by Halogen Bonding in the Design of Metal-Containing Arrays: Assembly of Double σ-Hole Donating Halolium with Cu^{I}-Containing O,O-Donors

Artem V. Semenov, Vadim Yu. Kukushkin, *et al.*
MARCH 31, 2023
INORGANIC CHEMISTRY
READ

Get More Suggestions >

https://doi.org/10.1021/acsomega.2c06729
ACS Omega 2023, 8, 6439−6454